PLASMA DYNAMICS

XVIII. PLASMAS AND CONTROLLED NUCLEAR FUSION*

A. Waves and Radiation

Academic and Research Staff

Prof. G. Bekefi
Prof. W. P. Allis
Prof. S. C. Brown
Prof. W. M. Manheimer
Prof. B. L. Wright
J. J. McCarthy
W. J. Mulligan
C. Oddou

Graduate Students

B. J. Becker
A. J. Cohen
L. Litzenberger
L. P. Mix, Jr.
L. D. Pleasance
G. L. Rogoff
C. E. Speck
N. E. Spithas
D. W. Swain
J. H. Vellenga

RESEARCH OBJECTIVES

The major goal of this group is to generate a basic understanding of various types of oscillations and waves in ionized gases that are relevant to problems in thermonuclear fusion and space research. The experimental and theoretical studies fall roughly into three main groups.

a. Investigations of electromagnetic radiation emitted spontaneously by the plasma, because of thermal and nonthermal fluctuations of the free charges. At present, particular attention is being paid to emission at long infrared wavelengths and to radiation generated as a result of many-body (collective) interactions between the charges.

b. Studies of the dispersion characteristics of small amplitude stable and unstable waves. We are now looking at the properties of ion and electron cyclotron oscillations, low-pressure striations, and ion sound waves.

c. Investigation of nonlinear plasma phenomena is one of our major goals for the next few years. In this connection, we are particularly interested in the properties of large-amplitude waves, particle trapping, nonlinear Landau damping, parametric coupling of three or more waves, and the coupling of waves with particles. The effects of boundaries and finite plasma geometry are considered.

We attempt to carry out these projects under well-controlled experimental conditions. This often entails the construction of new plasma sources. During the past year, for example, we have constructed two quiescent, collisionless, plasma facilities (PF 1 and PF 2) on which many of the studies described will be carried out.

G. Bekefi

1. CONSTRUCTION AND PROPERTIES OF A COLLISIONLESS, QUIESCENT PLASMA FACILITY (PF 1)

Using electron cyclotron heating in a mirror geometry, Lisitano and his co-workers[1] have produced an almost collisionless, quiescent plasma column that is useful in studying a variety of problems, such as wave propagation, instabilities, nonlinear

*This work was supported by the U.S. Atomic Energy Commission (Contract AT(30-1)-3980).

phenomena, and turbulence. In this report we describe the construction of a similar system (called PF 1) and the modifications that we have made to obtain a more uniform plasma column than that reported by Lisitano. In studying the plasma characteristics, we have used Langmuir probes. In Sections XVIII-C. 1 and XVIII-C. 2, we describe some optical and probe studies that were made on a facility (called PF 2) that differs essentially from PF 1 only in the over-all length of the machine.

Over-all System

This system, shown in Fig. XVIII-1, is made almost entirely of stainless steel. The backbone of the system is a stainless-steel tube, 5 inches in diameter, in which the plasma is generated and confined. This tube, 8 1/2 ft long, has an inside diameter of 4 3/4 inches. In the center of the tube, as well as at either end, are Tee-shaped manifolds which link the tube to 6-in. diffusion pumps, each of which is equipped with a gate valve and cryogenic trap. By using one of the end pumps with liquid nitrogen in the trap, base pressures of 2×10^{-7} Torr are obtainable, with pressures of 1×10^{-6} Torr obtainable after less than an hour of pumping.

Access to the interior of the system is via four, two-stage double O-ring seals and via two single O-ring seals. The double O-ring seals permit 1/2 in. polished stainless-steel tubes to be inserted into the system. The double O-ring seals are mounted in pairs on plates, 7 inches in diameter. In the present configuration one pair of seals is mounted at each end of the system on one of the arms of the Tee-shaped manifolds. The corresponding location on the center manifold is covered by a glass plate that provides an observation port for optical diagnostics. In order to move diagnostic probes at a uniform rate along the tube, one of the double seals has been equipped with a motor drive.

The center manifold, in addition to the observation port, has horizontal and vertical arms projecting radially from the axis of the tube. These arms are equipped with single O-ring seals. Care must be exercised in moving the Langmuir probes through these seals, which were used in obtaining the probe data presented in this report. These seals are also interchangeable with glass plates if desired for optical diagnostics.

The plasma is contained in the tube by an axial magnetic field, having mirror geometry at the ends. The power supplies for the straight section and mirror sections are completely independent, thereby providing a large range of mirror ratios. Both supplies provide current regulation within 0.05% after warmup, but their response to transients has a time constant of several milliseconds with a pure resistive load. The magnetic field is produced by 16 solenoids of major and minor diameters 13-1/2 in. and 7 in., respectively. The length of each solenoid is 4 1/4 inches. A typical field profile for measurements presented in this report is shown in Fig. XVIII-2. Also shown are the

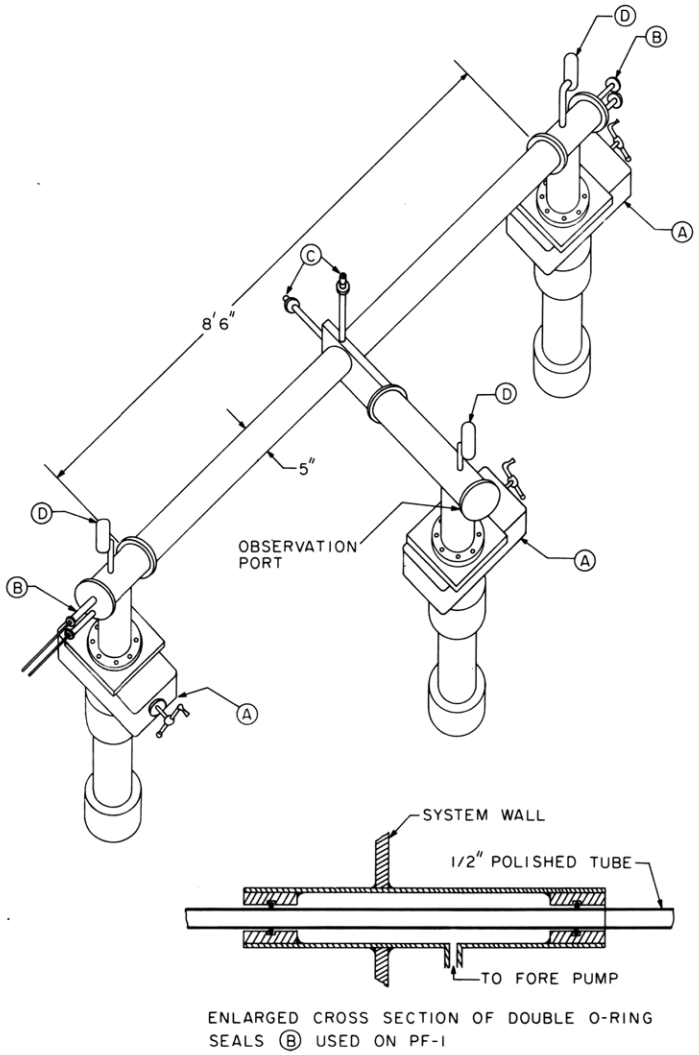

Fig. XVIII-1. Over-all view of system. (A) NRC, 6 in. diffusion pump with cryogenic trap and gate valve. (B) Two-stage double O-ring seal. (C) Single O-ring seal. (D) Ionization gauge.

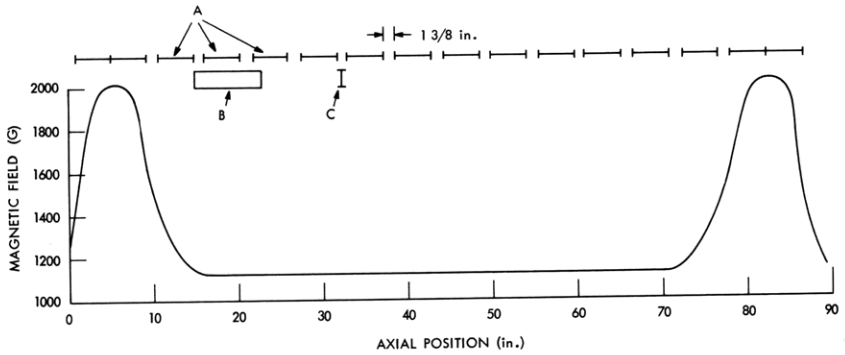

Fig. XVIII-2. Magnetic field vs position along the plasma column. (A) Positions of individual solenoid coils. (B) Position of the microwave structure used in producing the plasma. (C) Position of grid.

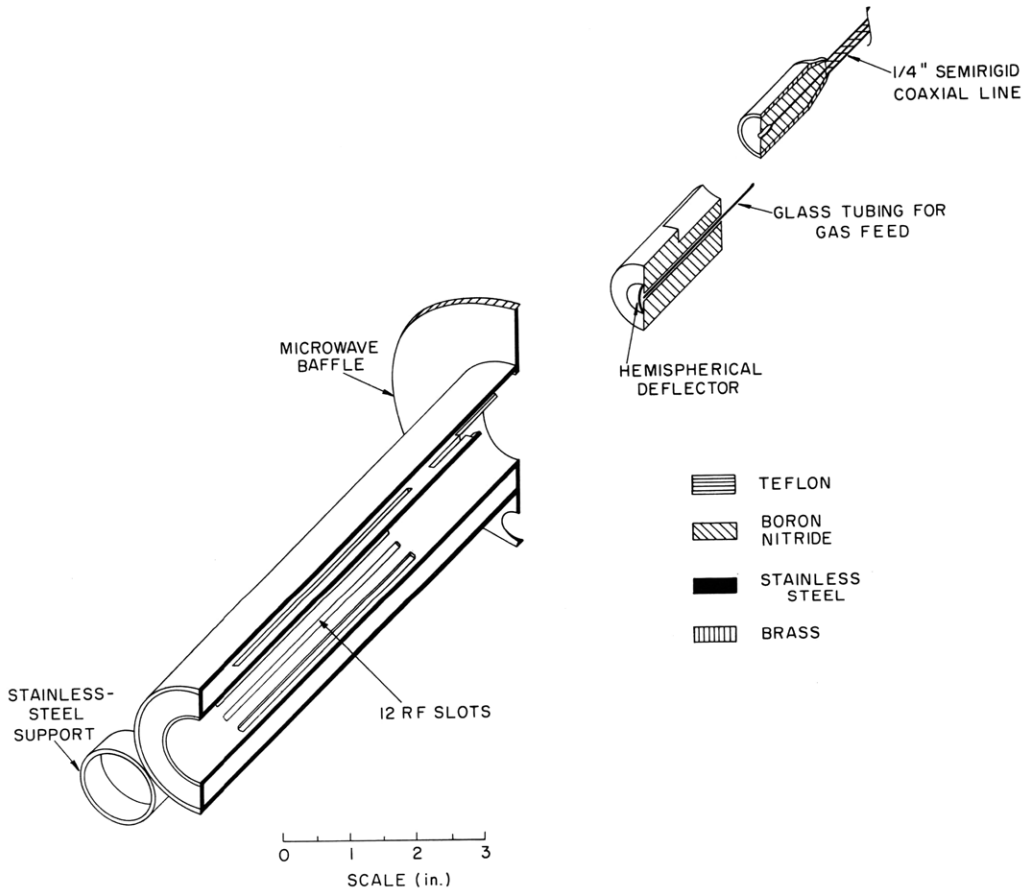

Fig. XVIII-3. Microwave structure used in the production of the plasma.

relative positions of the magnets, grid structure, and plasma generating device. Although compression of the scale masks the ripple, the uniformity of the center is approximately 0.5% rms.

Microwave Plasma Source

The plasma is generated by the structure shown in Fig. XVIII-3. This structure is similar to that of Lisitano,[1] the main difference being the substitution of unconnected slots for his continuous slot. To maximize the percentage of ionization, the gas is fed directly into the center of the structure. The boron nitride support, as well as the rear support of the structure, cause an order of magnitude pressure drop across the structure when only one diffusion pump is used. As noted in Fig. XVIII-2, the microwave structure is located in a region of relatively uniform magnetic field. Because of this and the necessity of operating at a frequency near the electron-cyclotron frequency, variations in the current of solenoid as little as 0.2% are sufficient to seriously degrade the plasma. The data presented in Section XVIII-C.1 were taken with an incident power to the structure of 28 W at a frequency of 3170 MHz.

In an effort to generate a plasma with a more uniform radial profile, a grid was added to the system. The relative position of the grid is shown in Fig. XVIII-2. The grid is made of 1-mil tungsten mesh and has 90% transmission. The grid is supported by a stainless-steel ring, 1 1/2 inch in diameter, which, in turn, slides on a boron nitride block.

Plasma Properties

The uniform cylindrical plasma column, approximately 1.5 m long and 3 cm in diameter, was studied in the midplane section of the machine, at a distance of ~40 cm from the microwave source. All measurements discussed here refer to a plasma made in Argon gas whose pressure in the main vacuum chamber was maintained at one of two values: 3×10^{-5} Torr and 3×10^{-6} Torr. In particular, we shall show the dramatic effects produced when a grid is placed between the microwave structure producing the plasma and the rest of the plasma column where the diagnostic studies were made.

A cylindrical Langmuir probe capable of radial displacement was used to determine the radial profile of electron density, temperature, and space (that is, plasma) potential. Figure XVIII-4a shows a typical recorder tracing of the voltage-current characteristics for a probe situated near the axis of the plasma column. Figure XVIII-4b is a plot of the logarithm of the electron current as a function of probe voltage used in determining the electron temperature. The electron current was deduced from the total probe current by subtracting the ion current obtained by a straight line extrapolation (shown dashed in Fig. XVIII-4a).

In Fig. XVIII-4b we see a straight line over almost two orders of magnitude in

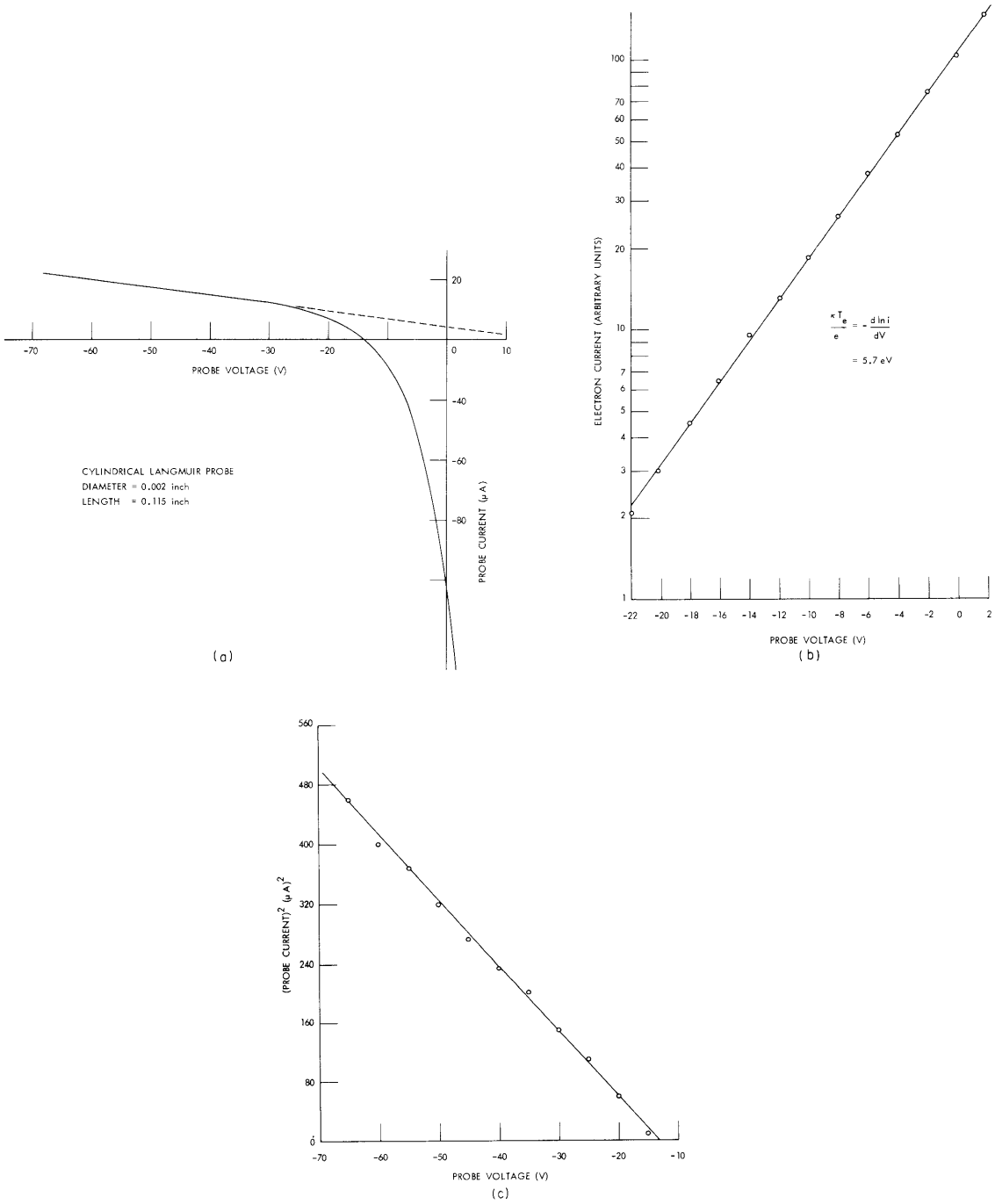

Fig. XVIII-4. (a) Recorder tracing of a Langmuir probe measurement made near the axis of the plasma column. No grid was placed in front of the microwave structure generating plasma.

(b) Determination of electron temperature from semilogarithmic plot of electron current against voltage. The points are taken from Fig. XVIII-4a.

(c) Determination of the space potential V_s and the electron density N from the ion current vs voltage taken from Fig. XVIII-4a.

electron current. This suggests strongly that the velocity distribution of electrons is close to a Maxwellian distribution. We wish to point out, however, that such good straight lines were found only for points at and near the axis of the plasma column at radial distances not exceeding 1 cm. At the visible rim of the plasma (corresponding to the rim of the RF structure producing the plasma), we observed pronounced breaks in the log I vs V curves, which suggest the presence of a colder plasma component. This non-Maxwellian nature may not be too surprising, in view of the fact that the plasma is in fact generated mainly in an annular region near the rim of the microwave structure.

The electron density and the space potential were determined from that part of Fig. XVIII-4a corresponding to the regime of ion collection. Since the probe radius was very small compared with the ion Larmor radius, theories for ion collection in the absence of a magnetic field should be applicable. Moreover, the probe radius was small compared with the electron Debye length, thereby permitting the use of Langmuir's orbital-motion theory.[2] According to this theory, the current I and the applied voltage V are related as follows:

$$I = 2\sqrt{2}\ \mathrm{erLN}\left[\frac{\kappa T_i}{M_i}\right]^{1/2}\left[1 - \frac{e(V-V_s)}{\kappa T_e}\right]^{1/2} . \qquad (1)$$

Here r and L are the radius and length of the probe, N is the ion density, T_i and T_e are the ion and electron temperatures, M_i is the ion mass, and V_s is the space potential (measured relative to ground potential). From Eq. 1 we see that I^2 should vary linearly with V, a fact that is borne out by experiment as is shown in Fig. XVIII-4c. The intercept of the straight line at I = 0 yields the space potential (T_e is known from Fig. XVIII-4b), and the slope of the curve gives the density N. The ion temperature was taken as 1 eV (see Sec. XVIII-C. 1), and for lack of more detailed knowledge, we assumed T_i to be independent of radial position within the plasma.

Figure XVIII-5 illustrates the radial profiles of N, T_e, and V_s for a plasma maintained at 3×10^{-5} Torr with no grid interposed in the plasma column. We see that all three quantities exhibit maxima at a position $r \approx 1.2$ cm, which is near the radial position where the plasma is presumably produced in the cylindrical microwave structure. The pronounced potential well at this radial position adds to our belief that the plasma is initially produced in an annular ring and ultimately diffuses inward to fill in the core. We see, however, a surprising result, namely that there is almost no outward radial diffusion; the plasma density decays within a distance of the order of one ion Larmor radius (for further details see Sec. XVIII-C. 2).

The strong radial variations of the plasma properties are undesirable characteristics for quantitative studies of wave propagation, instabilities, and so forth. Therefore we

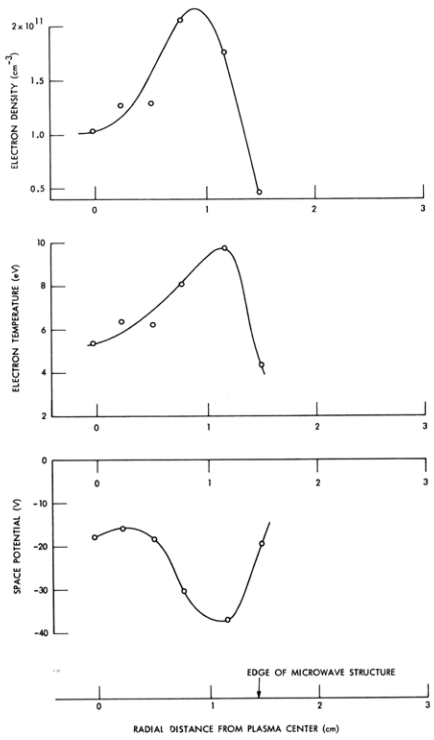

Fig. XVIII-5.

Radial profiles of N, T_e, and V_s in the Argon plasma column maintained at 3×10^{-5} Torr pressure. No grid is placed across the column.

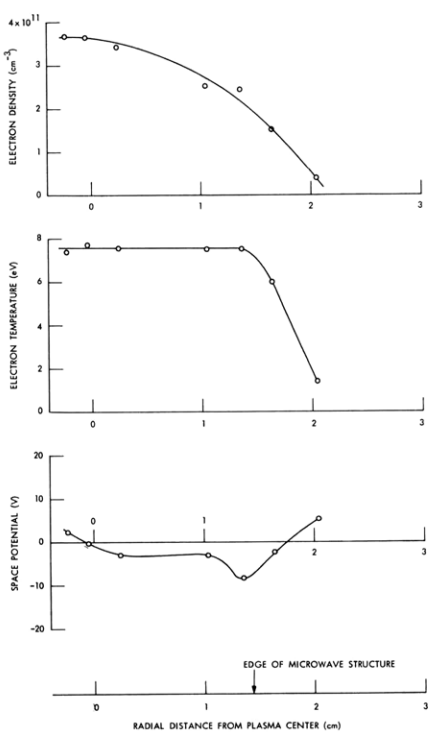

Fig. XVIII-6.

Same as Fig. XVIII-5, except that a grid is placed across the plasma column. The grid is biased 16 V negative.

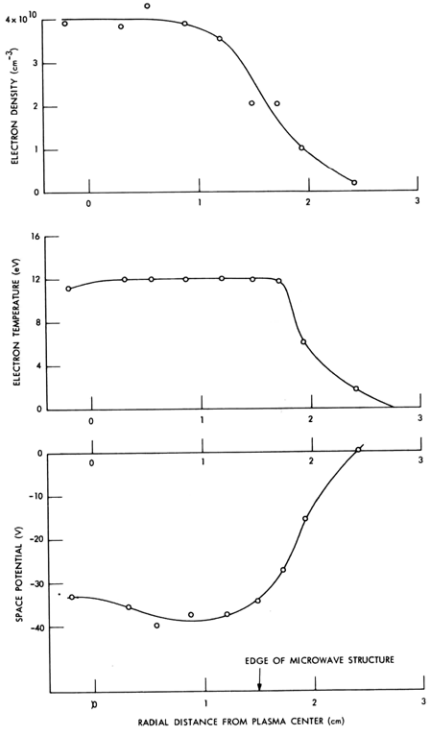

Fig. XVIII-7.

Radial profiles of N, T_e, and V_s in the Argon plasma column maintained at 3×10^{-6} Torr pressure. The grid is biased 4 V negative.

placed a metal grid across the plasma column which was capable of being biased positively or negatively with respect to V_s. We argued that such a grid tends to provide an equipotential surface and by shorting out the strong radial electric fields, the density and temperature variations may be reduced. Figure XVIII-6 shows that this indeed occurs. In Fig. XVIII-7 we show similar measurements made at ten times lower gas pressure (3×10^{-6} Torr). By lowering the gas pressure, the electron density fell by an order of magnitude and the electron temperature increased approximately 50%.

We find that we cannot maintain a steady-state plasma at pressures below 2×10^{-6} Torr with the available microwave power ($\lesssim$40 W).

The degree of quiescence of the plasma was observed with the Langmuir probe used as an RF antenna. The probe was biased negatively for studies of the ion density fluctuations, positively for electron density fluctuations, or it was maintained at floating potential to obtain some idea about electric-field fluctuations. At frequencies between 10 MHz and 10^{10} MHz the noise level was very low. At frequencies between 0 and 1 MHz the spectrum was essentially a monotonically decreasing function of frequency. We have not studied the frequency response of the probe and, therefore, some of the observed decrease is undoubtedly due to loss of sensitivity with increasing frequency. Some discrete noise structure was observed at low frequencies below ~50 kHz. An rms voltmeter with a frequency range of 10 Hz to 10^7 Hz was used in the measurement of the percentage of fluctuations in the ion and electron saturation currents to the probe ($(\Delta I/I)_{ion}$,$(\Delta I/I)_{electron}$) and in the floating potential fluctuations $e\Delta\phi/\kappa T_e$ (normalized to the electron energy). Table XVIII-1 lists the observations at the two pressures used in the experiments. The grid was in position in front of the microwave structure. Varying the bias on the grid had little effect on the percentage of fluctuations. The magnitude of the DC magnetic field along the column played an important role, and

Table XVIII-1. RMS fluctuations of the plasma in the frequency range 10 Hz-1 MHz.

Quantity	Gas Pressure	
	3×10^{-6} Torr	3×10^{-5} Torr
$\frac{e\Delta\phi}{\kappa T_e}$	0.2%	0.4%
$\left(\frac{\Delta I}{I}\right)_{electron}$	16%	2%
$\left(\frac{\Delta I}{I}\right)_{ion}$	20%	2.5%

the noise could be minimized by varying the magnetic field by less than 1 per cent. Table XVIII-1 gives values under optimum conditions. We see that at the lower pressures the noise fluctuations are quite substantial.

L. P. Mix, Jr., E. W. Fitzgerald, G. Bekefi

References

1. G. Lisitano, Proc. 7th International Conference on Ionization Phenomena in Gases, Vol. 1 (Gradevinska Kujiga Publishing House, Beograd, 1966); Appl. Phys. Letters 12, 32 (1968); also see G. Lisitano, R. A. Ellis, Jr., W. M. Hooke and T. H. Stix, Plasma Physics Laboratory Report MATT-Q-24, Princeton University, Princeton, N.J., 1966.
2. F. F. Chen, C. Etievant, and D. Mosher, Phys. Fluids 11, 811 (1968).

2. EXACT NONLINEAR COLLISIONLESS PLASMA WAVES II *

Arbitrary Zero

The nonlinear theory outlined in Quarterly Progress Report No. 88 (pages 121-129) (referred to as I) has been extended, principally by allowing the potential constant V_o (I, 1) to be arbitrary. This amounts to selecting some intermediate position between potential minimum ϕ_1 and potential maximum ϕ_2 at which the distribution becomes, periodically, exactly Maxwellian (Fig. XVIII-8). This alters the distribution function

$$f = \frac{n_o}{\sqrt{\pi}} e^{-(u+c)^2} = \frac{n_o}{\sqrt{\pi}} e^{-u^2-c^2} (\cosh 2uc - \sinh 2uc) \tag{1}$$

$$c = w\sqrt{1 - \phi/w^2}, \quad w = u - v$$

as shown in Fig. XVIII-9. The untrapped distribution oscillates across the Maxwellian distribution. Phase mixing symmetrizes the trapped distribution, thereby producing a discontinuity between the free and trapped distribution

$$f_t = \frac{n_o}{\sqrt{\pi}} e^{-u^2-c^2} \cosh 2uc. \tag{2}$$

The integration for the electron density n_1 is the same as before (I, 6)

$$n_- = n_o \sum_0^\infty M_a \phi^a / a!, \tag{3}$$

*This work was done partially while the author was Visiting Fellow at St. Catherine's College, Oxford University.

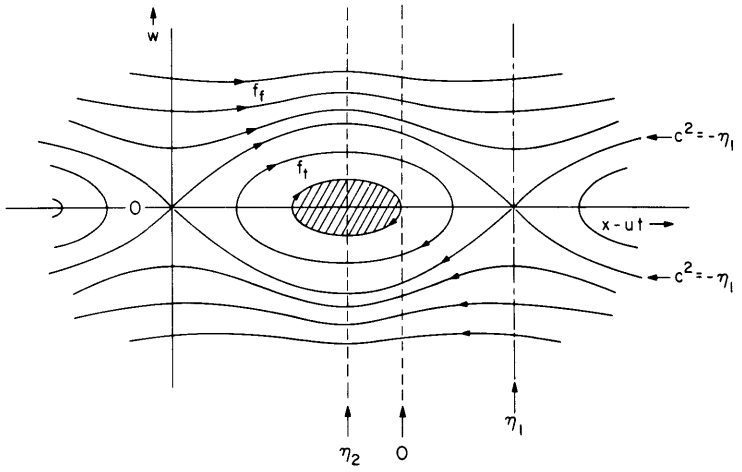

Fig. XVIII-8. Phase orbits.

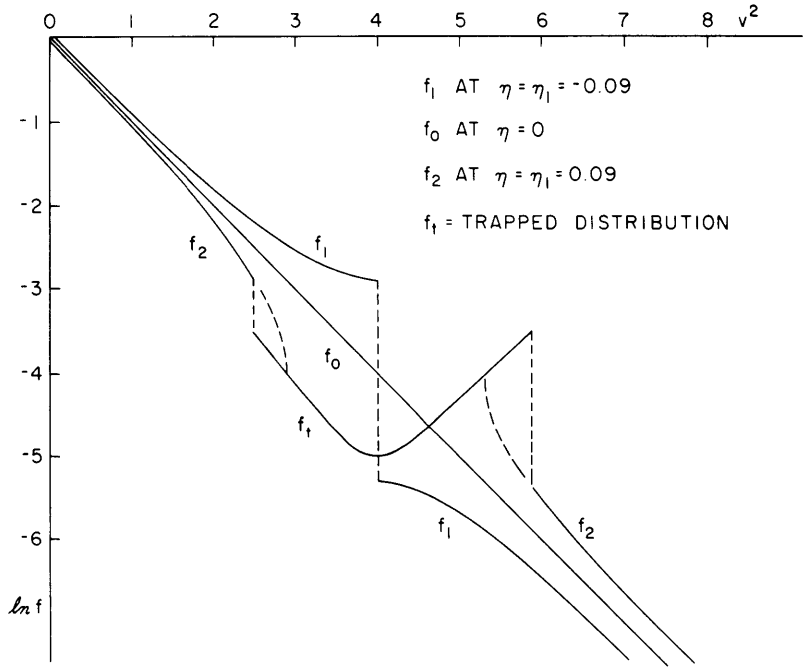

Fig. XVIII-9. Distribution function.

where

$$\left.\begin{aligned} M_o &= 1 \qquad\qquad M_1 = -\frac{1}{2}Z_r'(u) \\ 2aM_{a+1} &= (4a-1-2u^2)M_a + (1-2a)M_{a-1} \end{aligned}\right\} \tag{4}$$

are real confluent hypergeometric functions of $-u^2$. We may, however, proceed differently.

Landau Pole

It is noted that the Taylor expansion of the distribution (1),

$$f = \frac{n_o}{\sqrt{\pi}} e^{-v^2}\left[1 + \frac{v\phi}{w} + \frac{1}{2}\frac{\phi^2}{w^2}\left(v^2 + \frac{u}{2w}\right) + \frac{\phi^3}{2w^3}\left(\frac{v^3}{3} + \frac{vu}{2w} + \frac{u}{4w^3}\right)\cdots\right], \tag{5}$$

has a pole in first order, the Landau pole, and all higher orders are nonintegrable. In linear theory one neglects the higher orders and integrates around the Landau pole in the complex plane, the direction around the pole being determined by reasons of causality. This yields the first two terms of the series (3), but with the complex plasma dispersion function $Z'(u)$.

The function (1) has no poles but does have branch points at $w = 0$, $c = \pm\sqrt{-\phi}$. These are the reflection points of electrons at the sides of the potential wells. These branch points appear in the sinh 2uc, not in the cosh 2uc, term of (1) and phase mixing replaces them by the discontinuity at $c = \pm\sqrt{-\phi_1}$. Hence they do not influence the series (3). It is amusing, if nothing else, to proceed as in linear theory by keeping the sinh 2uc term,

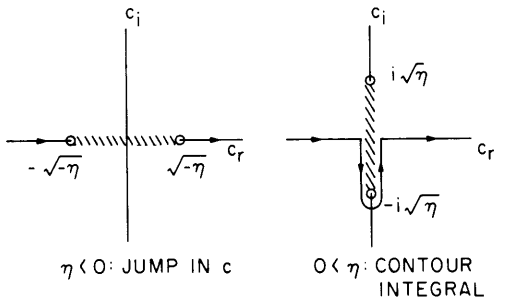

Fig. XVIII-10. Branch cut in the complex c plane.

making an analytic continuation to complex c, that is, into the shaded part of Fig. XVIII-8, and integrating around the branch cut to $-i\sqrt{\phi}$ (Fig. XVIII-10). This yields a set of complex functions M_{ac} in the series (3) of which the first one is given by (4) with the full complex dispersion function $Z'(u)$. This would yield the complete Landau theory,

and one may say that linearization produces the Landau pole from the confluence of two branch points. This also attributes Landau damping to the reflection of trapped electrons at the walls of the potential wells, more electrons being reflected from the back wall than from the front, because of the preponderance of electrons with negative w, which is expressed by the sinh 2uc term of (1). No meaning is given to the higher complex members of the series.

Resonant Current

Besides the modulated $n_-(\phi)$ there is a modulated flow $\Gamma(\phi)$ associated with the wave, and given by

$$\Gamma = \int_{-\infty}^{+\infty} fv\, dv = \int_{-\infty}^{+\infty} f(u+w)\, dw = n_- u + \int_{-\infty}^{+\infty} fc\, dc - \int_{-\sqrt{-n_1}}^{+\sqrt{-n_1}} fc\, dc$$

$$= (n_- - n_o)u + \Gamma_s = \Gamma_o + \Gamma_w + \Gamma_s. \tag{6}$$

The first term comes from the part of f that is even in w, the cosh 2uc part. The second term comes from the sinh 2uc part, and the third term subtracts the sinh 2uc for the trapped particles. The last is the flow induced by symmetrization. It is a necessary consequence of Landau damping and of the establishment of an undamped wave. The first two terms are in part fluctuating and in part direct. The fluctuating part Γ_w is a necessary accompaniment of the wave, but the direct part Γ_o is not necessary, and depends on the mode of excitation of the wave. In this theory it is determined by the location of the zero of potential. It is not an ordinary DC flow such as would be induced by a DC field, as it is carried by "resonant" electrons, not only the trapped electrons, whose velocity is close to the phase velocity of the wave. On account of space-charge neutrality, the average of n_- is n_+, hence

$$\Gamma_o = (n_+ - n_o)u. \tag{7}$$

Poisson's Equation

By writing

$$n_+ = n_o(1+C_2), \tag{8}$$

Poisson's equation integrates once to give the field

$$(E/2\omega_o)^2 = F = C_1 - C_2\phi + \sum_1^{\infty} M_a \phi^{a+1}/(a+1)! \tag{9}$$

and once again to give the phase

$$2\omega_o x = \int \frac{d\phi}{\sqrt{F}}. \tag{10}$$

In order to have a periodic wave, the field E, and hence F, must vanish at the minimum ϕ_1 and at the maximum ϕ_2 and F must be positive in between. Two possible situations are illustrated in Fig. XVIII-11. The constants C_1 and C_2 determine the field and slope at $\phi = 0$, but the possibility of two solutions depends, at least for small amplitudes, on the curvature, that is, on the sign of $dn_-/d\phi$.

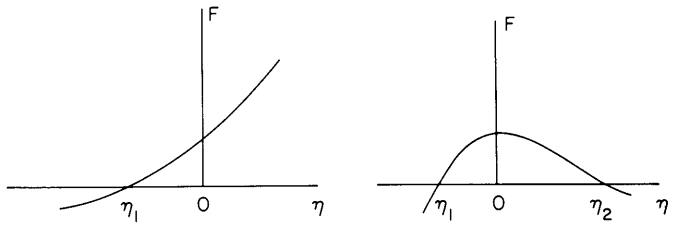

Fig. XVIII-11. Determination of wave amplitude.

There is only one zero when $dn_-/d\phi \geq 0$ because the electrons are then concentrated where the potential is positive and no sustained wave is possible. Self-consistency requires a negative potential to exist where the electrons are concentrated, that is, when $dn_-/d\phi < 0$, and then the two constants can always be adjusted in many ways to give two zeros, and sustained waves exist.

The constant C_1 raises the curve, thereby determining the amplitude $\phi_2 - \phi_1$, the constant C_2, which is proportional to Γ_o, tilts the curve and thus controls mainly the position of the zero of potential between ϕ_1 and ϕ_2. For zero current the point of zero potential must come where there is zero space charge, that is, at the level of the inflection point of the wave profile. The electron flow is in the direction of the wave when the inflection point is at a negative potential.

Slow Waves

It can be seen that

$$-(u+c)^2 = \phi - v^2 + 2u(w-c), \tag{11}$$

so that for slow waves, $u \ll 1$, the distribution (1) becomes Maxwell-Boltzmann. For this

distribution $dn_-/d\phi \approx n_- > 0$, and no sustained wave is possible. Landau damping will extinguish any wave that is started whose velocity is much less than thermal.

Cold Plasmas

The admission of an arbitrary V_o yields two-constant solutions, as compared with the one-constant solutions of report I. These two constants, denoted A and b, are related algebraically to C_1 and C_2.

The cold plasma limit has been solved, in part, by Akhiezer and Lyubarskii.[1] The distribution (1) is then a δ-function, and we can then write $c = -u$, which leads to

$$w^2 = \phi + u^2, \tag{12}$$

which merely expresses conservation of energy for an electron of energy u^2.

For $u \neq 0$, all electrons should be free, so, by continuity of current, n_-w = constant, or

$$n_- = \frac{n_o}{\sqrt{1 + \phi/u^2}}. \tag{13}$$

This expression can also be obtained from (3) in the limit $u \to \infty$, $\phi \to \infty$, ϕ/u^2 finite. Substituting in Poisson's equation and integrating, we obtain the following solution

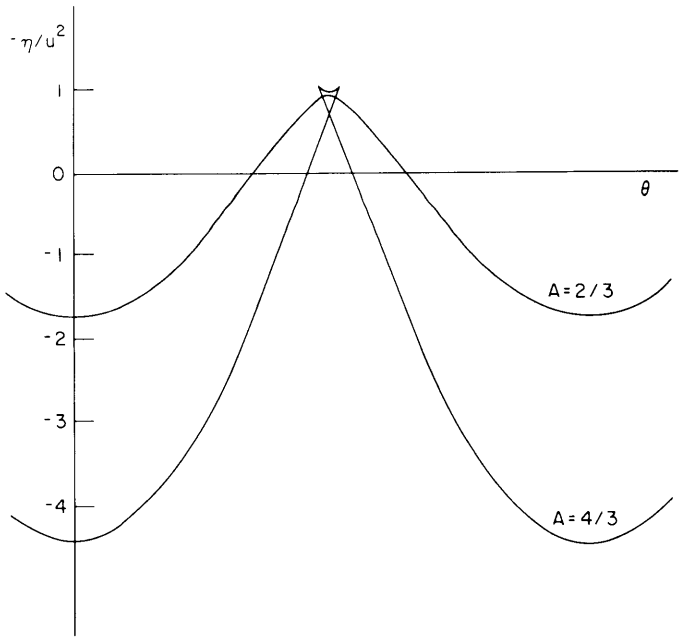

Fig. XVIII-12. Cold plasma waves. (The larger wave has broken.)

$$\phi/u^2 = b^2(1 + A\cos\theta)^2 - 1$$

$$n_+ = n_-(1 + A\cos\theta) = n_o/b \tag{14}$$

$$\omega_p x = bu(\theta + A\sin\theta)$$

expressed in terms of a phase angle θ. This wave is illustrated in Fig. XVIII-12. The constant b is related to C_2, and for no resonant current b = 1.

Substituting for x in terms of real time (I, 1) the fundamental frequency is seen to be

$$\omega = \omega_p/b, \tag{15}$$

which shows no dispersion, but a Doppler shift if there is a current.

The amplitude A produces phase modulation, and for $A \geq 1$, $dx/d\theta = 0$ at some phases. This represents overtaking, and when this happens the potential given by (14) becomes double-valued, which is unacceptable. A = 1 represents a maximum amplitude. Above this amplitude stationary electrons are trapped by the wave.

Linear Limit

Neglecting ϕ^2 and higher terms in (3), we find that

$$\phi = A\sin\omega x/u + b$$

$$n_+ = n_o(1+bM_1) \tag{16}$$

is a solution, with the dispersion relation

$$\frac{\omega^2}{\omega_p^2} = \frac{-2u^2M_1}{1 + bM_1} = -2u^2M_1\left(1 - \frac{\Gamma_o}{n_+u}\right). \tag{17}$$

With no resonant flow the dispersion is exactly the Vlasov dispersion. It allows for waves only when M_1 is negative, that is, for

$$u^2 > 0.857. \tag{18}$$

Slow waves cannot be sustained, as has already been noted.

The additional constant b modifies the dispersion exactly in the manner of van Kampen's "modes."[2] The effect found here, however, is not due to an independent wave mode but to a peculiarity in the excitation mechanism by which the average potential in the wave differs from that in the plasma into which it propagates.

W. P. Allis

References

1. A. I. Akhiezer and G. Ya. Lyubarskii, Dokl. Akad. Nauk SSSR 80, 193 (1951).
2. K. M. Case, Ann. Phys. 7, 352 (1959).

3. STRIATIONS IN A LOW-PRESSURE DISCHARGE

In Quarterly Progress Report No. 91 (pages 82-104) I described an experiment for studying striations in a low-pressure Argon discharge and the theory that was being developed to explain the observations. In this report, some modifications of the theory will be presented and the results obtained thus far will be given.

Changes and Additions to the Theory

a. Ion Equations

The fluid equations for ion motion differ from work previously presented[1] by including the effect of axial drift of the ions attributable to the DC axial electric field. With this effect included, the equation of conservation of momentum is

$$(-i\omega+ikV_{z+}+\nu_+)MN_+v_z = -ikT_+n_+ + qN_+e_z. \tag{1}$$

Then the equations of continuity of ions and metastables can be combined with Eq. 1 to yield

$$[1-i(\omega-k\mu_+E)\tau_+]\,\frac{n}{N} + \frac{ik\mu_+E\tau_+}{1 - i(\omega-k\mu_+E\tau_+)/\nu_+}\,\frac{e}{E} = \frac{s_m}{S_m(1-i\omega\tau_m)} + \frac{s_i}{S_i} + \frac{\delta\tau_+}{\tau_+}. \tag{2}$$

The symbols have been defined previously.[2]

Now define dimensionless frequency and wave numbers s and p by

$$s = \omega\tau_+$$

$$p = kR.$$

Let

$$c_1 = \mu_+E\tau_+/R$$

$$c_2 = (\nu_+\tau_+)^{-1}$$

$$c_3 = \tau_m/\tau_+,$$

and define $G_1(p)$ through $G_4(p)$ by

$$\frac{n}{N} = G_1(p)\,\frac{e}{E}$$

$$\frac{s_m}{S_m} = G_2(p)\,\frac{e}{E}$$

$$\frac{s_i}{S_i} = G_3(p)\,\frac{e}{E}$$

$$\frac{\delta T}{T} = G_4(p)\,\frac{e}{E}.$$

It has been shown[3] that $\frac{\delta\tau_+}{\tau_+} = -\frac{\delta T}{2T}$. Then Eq. 2 may be written

$$[1-i(s-c_1p)]G_1(p) + \frac{ic_1p}{1 - ic_2(s-c_1p)} = \frac{G_2(p)}{1 - ic_3s} + G_3(p) - \frac{G_4(p)}{2}. \tag{3}$$

The functions $G_n(p)$ will be obtained from the electron equations. Once these functions are known, Eq. 3 is a dispersion relation that may be solved for s as a function of p.

b. Electron Equations

The electron equations for the time-variant (or AC) part of the electron distribution function are the same as those given previously,[4] except for an algebraic error, which consisted of the omission of a factor x multiplying the first term of Eq. 42. Eliminating y^1 gives an inhomogeneous equation for y^0 of the form

$$\frac{d^2y}{dx^2} + a(p,x)\frac{dy}{dx} - b(p,x)\,y = D(p,x)\,\frac{e}{E}, \tag{4}$$

where now $y = y^0$, the dimensionless electron distribution function

$$a = \Omega(x) - i2phx$$

$$b = p^2h^2x^2 + iph(1+x\Omega(x)) + \frac{\nu_c(x)}{3\nu_a^2}\left[\nu_{ex}(x)+\nu_i(x)+x\nu_L S(x-x_w)\right]$$

$$D = (iphx-2\Omega(x))\frac{dY}{dx} - \frac{2d^2Y}{dx}$$

Y = dimensionless DC distribution function

$$\Omega(x) = \frac{d}{dx}\ln\left[\frac{x^2}{\nu_c(x)}\right]$$

$$h = \nu_L/\nu_a.$$

Equation 4 is an inhomogeneous differential equation for y(x), with p, the dimensionless wave number, as a parameter. From the right-hand side of Eq. 4, it is seen that y is proportional to e/E, which is the AC electric field divided by the DC field. If, for computational purposes, e/E is set equal to one before solving for y, then the values of $\frac{n}{N}$, $\frac{s_m}{S_m}$, $\frac{s_i}{S_i}$, and $\frac{\delta T}{T}$ computed from y,[5] will be exactly G_1, G_2, G_3, and G_4, respectively.

Solution of the Electron Equations

Equation 4 has complex coefficients that also depend on the independent variable x. Physically, the only boundary condition that can be placed on y is that it be normalizable; that is,

$$4\pi \int_0^\infty y(x)\, x^2\, dx$$

must be finite. This condition implies that $\lim_{x\to\infty} y(x) = 0$, and $\lim_{x\to 0} y(x) < \frac{M}{x^3}$, where M = constant.

Equation 4 has been solved numerically for values of E, p, ν_c, etc., corresponding to the actual experimental situation in an Argon discharge.[6] Figure XVIII-13 shows the result of this calculation for a value of p = 1.0. In this figure, the distribution function has been represented in polar form

$$y = |y|\, e^{i\theta}.$$

In Fig. XVIII-13a log $|y|$ is plotted against x, and in Fig. XVIII-13b θ against x. These curves show considerable structure with pronounced cusps at values of x of 3.1-3.3 and 4.4-4.5. Since x is in "square-root volts," these values of x correspond to energies of 10.2 and 20 eV. These energies correspond approximately to the first excitation potential of Argon (x = 3.28) and the calculated potential of the wall (x = 4.35). These cusps are attributed to a large change in the driving term, since Y' and Y" change abruptly at these points.

It can be seen from Fig. XVIII-13 that y(x) tends to spiral around the origin for large values of x. This behavior can also be seen in an asymptotic analytic solution to the problem, and appears to be correct.

Evaluation of Macroscopic Parameters from y(x)

The values of $G_n(p)$ can be computed by integrating the distribution function times an appropriate multiplier over all speeds. For example,

$$G_1(p) = 4\pi \int_0^\infty y(p,x)\, x^2\, dx.$$

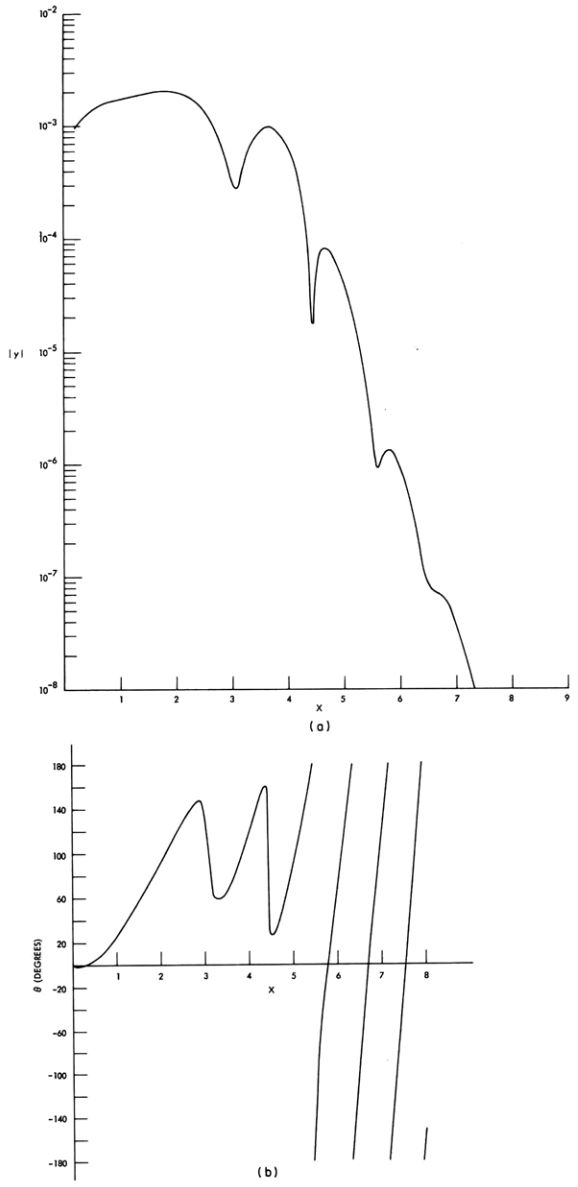

Fig. XVIII-13. AC distribution function $y(x) = |y(x)|\, e^{i\theta(x)}$.
(a) Log |y| vs x. (b) θ(x) vs x.

Now $G_1(p)$ is merely the fractional density perturbation divided by the fractional electric field perturbation, as defined previously in this report. The bulk of the electrons are in the low-energy part of the DC distribution function. The low-energy portion of Y(x) (below x = 3) looks very much like a Maxwellian, with an effective temperature of ~6.5 eV as measured directly. Therefore an approximate solution for the density perturbation can be obtained by assuming a Maxwellian distribution with this temperature, and using the fluid equations for the electrons.

In this simple theory it is assumed that the electrons are in exact thermodynamic equilibrium with the spatial electric fields, and the effects of inelastic collision may be neglected. Then the electron conservation equation

$$\frac{\partial n}{\partial t} = D_- \nabla_n^2 + \mu_- \left[N \frac{\partial e}{\partial z} + E \frac{\partial n}{\partial z} \right] + \text{ionization term}$$

becomes

$$0 = -k^2 D_- n + ik\mu_- [Ne + En].$$

Assume $\frac{D}{\mu} = \frac{T}{q}$ for a Maxwellian, which yields

$$\frac{n}{N} = \frac{-1}{1 + ik\, l_e} \frac{e}{E_o}$$

or

$$G_1(p) = \frac{-1}{1 + i \frac{l_e}{R} p}, \tag{5}$$

where

$$l_e = \frac{T}{qE_o} \approx \frac{6.5 \text{ volts}}{1 \text{ v/cm}} = 6.5 \text{ cm},$$

so that

$$\frac{l_e}{R} = \frac{6.5}{1.8} = 3.6.$$

From Eq. 5, it is seen that $-[G_1(p)]^{-1} = 1 + i \frac{l_e}{R} p$. Then the computed values of $G_1(p)$ should look something like this if the computer program and the complete theory are correct. Figure XVIII-14 shows a plot of the real and imaginary parts of $-[G_1(p)]^{-1}$. It can be seen from the graphs that

$$-[G_1(p)]^{-1}_{\text{computed}} = 0.38 + i3.8p.$$

Therefore, the computed values and the simple fluid model agree rather well with regard to the imaginary part, but the real parts are different by a constant factor of approximately 2.5. This discrepancy may be due to either the simplicity of the fluid model or numerical errors in the computation.

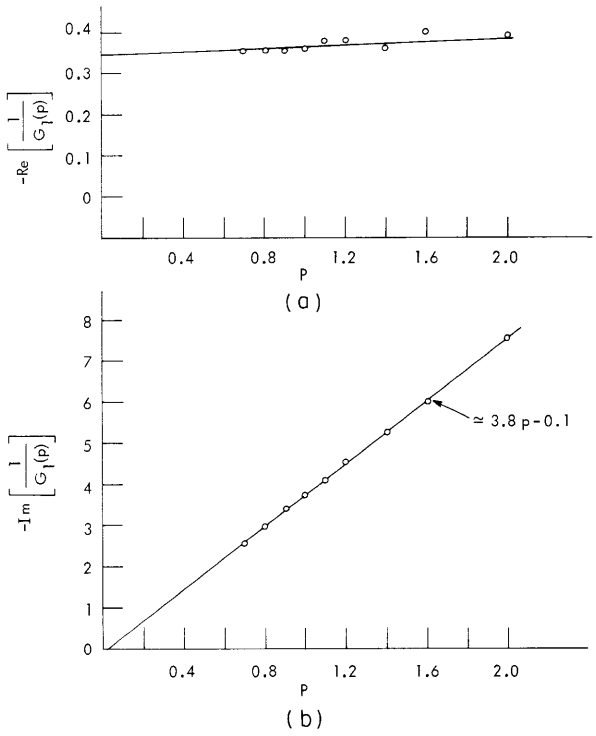

Fig. XVIII-14. $[G_1(p)]^{-1}$. (a) Real part. (b) Imaginary part.

There is no way to get a decent analytic solution for G_2, G_3 or G_4, since these terms are strongly dependent on the tail of y(x). Unfortunately, it is just these terms that enter strongly into the dispersion relation for striations.

Solutions to the Dispersion Relation

In the limit of zero ionization ($G_2=G_3=0$), the use of Eq. 5 for the electrons and Eq. 2 for the ions (with the right-hand side of (2) set equal to zero) yields the usual dispersion relation for ion acoustic waves in a homogeneous plasma, with an ion drift in the axial direction and elastic collisions included. This relation is of the form

$$\omega = kV_+ - \frac{i\nu_+}{2} \pm \sqrt{k^2u_a^2 - \frac{\nu_+^2}{4}}$$

$$\omega \approx kV_+ \pm ku_a - \frac{i\nu_+}{2}$$

for $2ku_a \gg \nu_+$, where

$$u_a^2 = \frac{T}{M}. \tag{6}$$

Thus, when G_2, G_3, and G_4 are set equal to zero, the computed dispersion relation should equal the simple relation in Eq. 6.

Figure XVIII-15 gives a plot of the computed ν against p for p real. The dashed line is for no inelastic collisions, and is very close to the curves computed from Eq. 6.

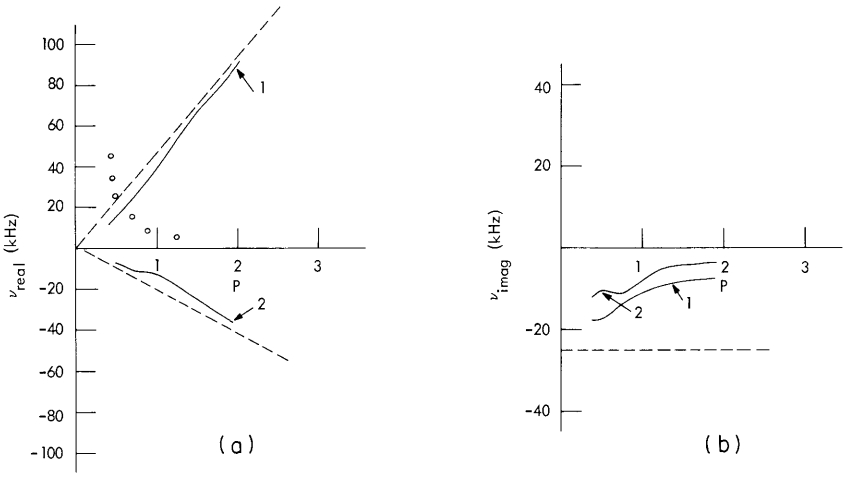

Fig. XVIII-15. Dispersion relation of waves. Dashed lines are computed curves for $G_2 = G_3 = G_4 = 0$. These correspond to the usual ion acoustic waves. Solid lines are for $G_2 \ldots G_4 \neq 0$. Note that damping (Im ν) has decreased in magnitude, but the real part still predicts a forward wave. (a) Real part of ν vs p. (b) Imaginary part of ν vs p. Circles are experimental points.

The solid curves represent the dispersion relation obtained when the inelastic terms are included. Note that the damping of the wave has been decreased considerably, but that the computed values for the real part of the ν-p curve still predict a forward wave, in disagreement with experiment. The circles show the experimentally measured values of ν vs p in the discharge.

In summary, the usual theory used to explain striations at high pressure has been extended in a straightforward manner to a low-pressure regime. The theory and experiment do not agree yet. Work will continue to try to resolve this disagreement.

D. W. Swain

References

1. D. W. Swain, Quarterly Progress Report No. 91, Research Laboratory of Electronics, M.I.T., October 15, 1968, pp. 82-104, see p. 87, Eqs. 11-16.

2. Ibid., pp. 85-86.

3. Ibid., p. 90.

4. Ibid., p. 98, see Eqs. 42 and 43.

5. Ibid., pp. 98-99, see Eqs. 45-48.

6. Ibid., p. 83.

XVIII. PLASMAS AND CONTROLLED NUCLEAR FUSION*

B. Diffusion and Turbulence

Academic and Research Staff

Prof. T. H. Dupree
Prof. L. M. Lidsky
Prof. W. M. Manheimer

Graduate Students

K. R. S. Chen
H. Ching
S. I. Friedman
H. R. Greenberg
J. N. Hamawi
P. M. Margosian
C. K. McCormick
R. L. McCory, Jr.
M. Murakami
L. C. Pittinger
J. E. Robinson

RESEARCH OBJECTIVES

1. Differential Cross-Section Measurements

Techniques developed in magnetic-mirror experiments can be applied to the rapid and accurate measurement of differential scattering cross sections. The main feature in this experiment is the use of the mirror fields, rather than slits or edges, as angle-discriminating elements. The result is the ability to use the total azimuthally integrated scattering from a line source as the scattering signal, thereby improving both sensitivity and the signal-to-noise ratio. The experiment will be performed for electron-atom scattering, but the experimental method will also be applicable to ion-atom scattering. The ultrahigh vacuum system ($\sim 10^{-9}$ Torr) and magnetic field sources for the electron experiment have been completed.

L. C. Pittenger, L. M. Lidsky

2. Fusion-Fission Reactors

Calculations show that a fusion reactor of moderate size could be built that would yield tritium breeding ratios in excess of 1.35. This, in effect, would free at least 0.10-0.15 neutrons per fusion reaction to be used for other purposes. A possible use is as input to a marginal fast breeder or advanced converter fission reactor. This symbiosis would act to eliminate the major weaknesses of both power-producing schemes, that is, the low power density of fusion reactors and the long doubling time of breeder reactors.

L. M. Lidsky

3. Toroidal Nonadiabatic Experiment

Our original experiment for measuring the lifetime of electrons circulating in a toroidal magnetic trap has been completed. The technology needed to inject electrons into the trap and to measure their lifetime has been perfected. Using this apparatus, we have verified the half-integral dependence of diffusion coefficient upon field strength

*This work was supported by the U.S. Atomic Energy Commission (Contract AT(30-1)-3980).

and have been able to estimate the lifetime of dissociated molecules in nonadiabatic corkscrew injectors. We are attempting to see if this experiment can be improved by correcting the causes of the long-term magnetic field drifts that limited electron lifetime to $\lesssim$200 transits. Minor modification to the vacuum system may also become necessary if the electron path length is appreciably extended.

P. M. Margosian, L. M. Lidsky

4. Incoherent Scattering – Anisotropic Velocity Distributions

We plan to use incoherent scattering techniques to measure the distribution of plasma electron velocities in the directions parallel and perpendicular to the confining magnetic field. Experiments show that the electron temperature in the HCD plasma is anisotropic and that the degree of anisotropy depends on several plasma parameters. Our first aim is to determine whether thermalization is caused by classical (Coulomb) scattering or by wave-particle interactions. Our experience in similar experiments indicates that the use of a 100-MW Q-switched laser will allow determination of the velocity distribution function with 5% accuracy out to 3 T_e or so. If this turns out to be the case, we shall go on to create distribution function anomalies and study the effect of their magnitude on instability growth rates. This will enable direct experimental verification of present marginal stability theories.

G. K. McCormick, L. M. Lidsky

5. Coherent Scattering from Steady-State Plasmas

We are attempting to observe coherent scattering of 10.6 μ radiation from the moderate density steady-state plasma produced by the hollow-cathode discharge source. Our goal is the comparison of the experimentally measured and theoretically predicted scattered spectra in order to determine the spectrum of plasma density fluctuations, that is, to measure plasma turbulence. We are using a 100 W N_2-CO_2-He laser as a radiation source and solid-state detectors. The experiment, thus far, has been plagued by very low signal-to-noise ratios, but recent work shows that cooling all surfaces in the optical path to 77°K increases the "detectivity" of the system by more than a factor of six. This change plus the use of a narrow-band optical filter at 4.2°K should allow the resolution of the detailed shape of the scattered spectrum in the plasma frequency "wings." If this is successful, we plan to increase the turbulence level in the plasma and observe the spectral changes.

K. R. S. Chen, L. M. Lidsky

6. Nonadiabatic Scattering Experiment

An apparatus has been constructed in which electrons can be trapped for long periods of time and caused to interact many times with arbitrarily chosen magnetic field perturbations. The electrons are trapped in a high vacuum region between gated electrostatic "mirrors." Existing apparatus has been modified to produce the good vacuum required ($\sim 10^{-8}$ Torr), and requisite high-voltage pulsed trapping and timing circuitry (for example, 1800-V flat topped pulses with 5×10^{-9} sec rise time) has been developed and tested. The theory of nonadiabatic scattering from resonant and near-resonant helical magnetic field perturbations has been extended and made more rigorous. The goal of this work is an improved understanding of wave-particle scattering phenomena in laboratory and astrophysical plasmas. There appears to be application also to the study of nonlinear wave growth.

M. Murakami, L. M. Lidsky

7. External Multipole Design Study

We wish to study magnetic flux surfaces and particle orbits for a toroidal modification of the linear multipole plasma confinement geometry. In the particular case of greatest interest to us, the plasma would be mirror-confined to the region inside the multipoles (that is, the plasma "behind the bars" would be lost). This configuration has many interesting properties and might be suitable for eventual construction at M. I. T. The first step in our study will be the development of flux surface and particle orbit computer codes that are well-suited for use on the time-shared computer system.

L. M. Lidsky

1. SINGLE ROTATIONAL MODE CO_2 LASER

With the usual scheme of using a gold-coated mirror and a germanium flat (with antireflective coating at the second surface) as CO_2 laser end mirrors, the output of the laser is multimode, usually centered at 10.5912 μ, accompanied by either 10.5713 μ or 10.6118 μ radiation or other rotational modes. Furthermore, the output for each mode is unstable and the transfer from one mode to the other occurs frequently (the time of transfer is of the order of seconds). We have replaced the germanium flat by a Fabry-Perot etalon and find that the output can be limited to a single stable mode. The power of this single-mode output now is only half of that of the previous multimode value. We are still seeking to optimize the output power by changing parameters of the discharge. The reflectivity[1] of the Fabry-Perot etalon is

$$R_{FP} = 1 - \frac{\tau}{\left[1 + \frac{4R}{(1-R)^2} \sin^2\left(\frac{2\pi t}{\gamma} \cos i\right)\right]},$$

where $\tau = \left(\frac{T}{1-R}\right)^2$, γ is the wavelength of the incident light in the medium between the two plates, t is the distance between the two plates, R and T are the reflectance and transmittance of the semireflecting plates, respectively, i is the incident angle of the

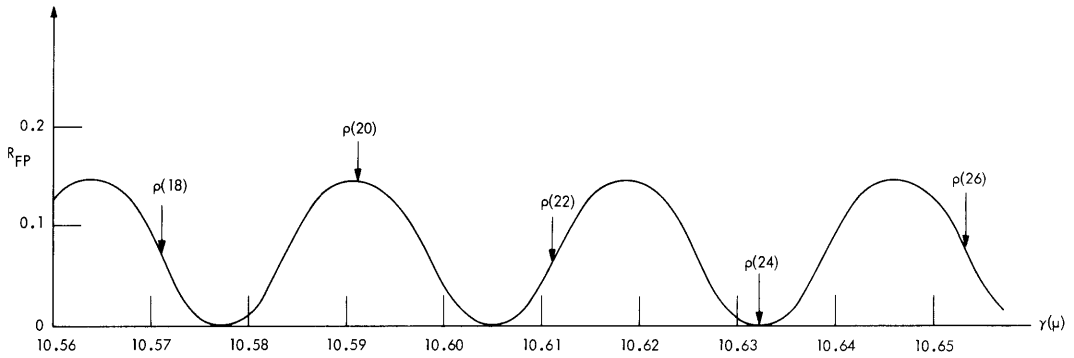

Fig. XVIII-16. Fabry-Perot reflectivity vs wavelength. Arrows indicate wavelength of the rotational modes.

light. In our case, the light incidents normally, the plates are NaCl flats, the medium is air; therefore, for a 10.6 μ laser, $\tau = 1$, $R = 0.039$, $i = 0$, $0 \leq R_{FP} \leq 0.145$. The maximum Fabry-Perot reflectivity (0.145) is near the optimum value for a 3-m laser.

If we choose the thickness t so that R_{FP} is large for one mode of the laser and is very small for other high-gain modes, it is possible to make the laser oscillate in one mode. We choose the thickness t(=0.08076 in.) to be the 387^{th} order of 10.5912 μ, and the reflectivity vs wavelength, γ, is shown in Fig. XVIII-16.

K. R. S. Chen, L. M. Lidsky

References

1. P. Jacquinot, J. Opt. Soc. Am. 44, 761 (1954).

XVIII. PLASMAS AND CONTROLLED NUCLEAR FUSION*

C. Plasma Diagnostics

Academic and Research Staff

Prof. G. Bekefi
Prof. B. L. Wright

Graduate Students

E. V. George
J. K. Silk

RESEARCH OBJECTIVES

The aims of this group are to perfect and refine existing methods of studying the properties of plasmas and, in particular, to devise novel techniques. At present, we are concentrating on the following studies. (a) An optical study of line spectra that is being used in determining the temperature of ions. (b) Measurements of the electron velocity distribution functions from the spectrum of the microwave emission of collective Bremsstrahlung. (c) A high-resolution Michelson interferometer utilizing a laser as the source, for use in the determination of electron concentrations in plasmas.

G. Bekefi

1. OPTICAL MEASUREMENTS ON THE PLASMA FACILITY II (PF 2) ARGON PLASMA

Introduction

This report presents some preliminary results of optical spectrometric measurements of the ion temperature in the Argon plasma generated in the apparatus designated Plasma Facility II (PF 2). Data on the ion temperature are sought to provide a more complete picture of the energetics of the plasma. An estimate of the ion temperature is also necessary for the determination of the electron density from Langmuir probe data presented in Section XVIII-A. 1 and Section XVIII-C. 2.

The PF 2 plasma apparatus is similar to that of PF 1 (described in Section XVIII-A. 1), with the following exceptions: (a) the length of PF 2 (115 cm) is approximately half of that of PF 1; (b) the longitudinal slots in the Lisitano structure of PF 2 are connected with short azimuthal slots at the ends to form a continuous slot, shaped like a square wave wrapped around the cylindrical structure. In PF 1 the azimuthal slots have been shorted out; (c) PF 2 does not have a grid like that added to PF 1 for some of the measurements.

*This work was supported by the U. S. Atomic Energy Commission (GK-2581).

Optical Apparatus

The objective of the optical measurements is to determine the ion temperature from measurements of the Doppler breadth of an ion emission line. The measurement utilizes a pressure-swept Fabry-Perot interferometer patterned on a design of Biondi.[1] The instrument employs a 0.5-cm spacer like that described by Phelps[2] and $\lambda/50$ plates, 2 inches in diameter, with broadband dielectric coatings. The finesse and resolving power are 30 and 5.46×10^5 (at 5000 Å), respectively, determined by measurements made with a single-mode laser. In the measurements made, thus far, the plasma is viewed transversely through a flat window. (Observations in the direction parallel to the field are also planned.) The light is collected by a lens at focal length from the center of the plasma. Since the radius of the plasma is comparable to the ion Larmor radius, it is assumed that the ion temperature is independent of radius and no attempt is made to obtain space-resolved measurements. An interference filter with 5 Å bandwidth is tuned by rotation to transmit the Argon ion line, 4610 Å. A polarizing filter with its axis parallel to the magnetic field transmits only the Zeeman π components of the line and eliminates the σ components. The Zeeman splitting of the π components is negligibly small (10^{-3} Å) for the 1000-G field applied to the plasma in these measurements. The fringe pattern formed by the interferometer is focussed on a screen containing a pinhole, 0.015 inch in diameter. The pressure scanning is accomplished by slowly admitting Argon from a high-pressure reservoir into the initially evacuated chamber housing the instrument so that the pressure rises essentially linearly with time. The light transmitted by the pinhole during the scan is detected by a liquid-nitrogen-cooled photomultiplier. The output of the photomultipler is displayed on an X-Y recorder, with the x axis time swept to yield a direct record of intensity as a function of wavelength. The wavelength calibration is obtained from a knowledge of the free spectral range of the interferometer by scanning through two complete fringes. Further details on the interferometer system are available in a previous report.[3]

Results of Preliminary Optical Measurements

This phase of the experimental effort is still at the "work-in-progress" stage. Further measurements are under way to confirm the initial results and to determine the variation of ion temperature with plasma conditions. The data that have been obtained have led to a pro tempore adoption of roughly 1 eV for the ion temperature under typical conditions.

A typical X-Y recorder trace of the interferometer system output is shown in Fig. XVIII-17. This measurement was made at a pressure of 3.8×10^{-5} Torr and excitation power of 49 W. The main field was 1100 G, and the mirror ratio was 1.6. The

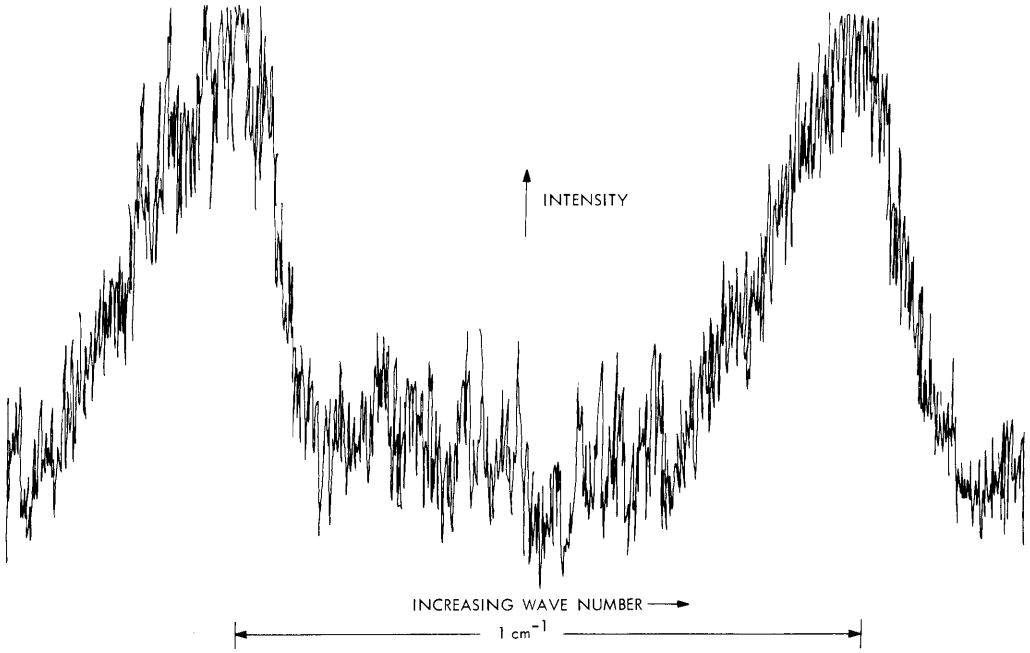

Fig. XVIII-17. Typical interferometer output.

observed breadth of the line in this case is 0.261 cm^{-1} which corresponds to a Doppler width of 0.222 cm^{-1} after correction for the instrumental breadth. The value of the ion temperature is 0.84 eV. In view of the experimental uncertainties, this value is not significantly different from 1 eV.

The origin of the asymmetry of the line has not yet been identified. The possibility that it is due to azimuthal motion of the plasma is being considered in the further study of ion temperature.

J. K. Silk

References

1. M. A. Biondi, Rev. Sci. Instr. 27, 36 (1956).
2. F. M. Phelps III, J. Opt. Soc. Am. 55, 293 (1965).
3. J. K. Silk, Quarterly Progress Report No. 88, Research Laboratory of Electronics, M.I.T., January 15, 1968, pp. 149-152.

2. LANGMUIR PROBE MEASUREMENTS ON A HELIUM PLASMA IN PLASMA FACILITY II (PF 2)

Introduction

This report describes some of the characteristics of a Helium plasma generated in the PF 2 apparatus. The discussion includes estimates of the mean-free paths and the results of Langmuir probe measurements of electron density, temperature, and space potential as a function of radius and externally controlled plasma conditions. The probe data are qualitatively similar to the measurements in the Argon plasma studied in PF 1 (described in Sec. XVIII-A. 1).

Estimates of Parameters Describing the Helium PF 2 Plasma

Table XVIII-2 lists some estimates of the magnitudes of the parameters describing the plasma. The estimated quantities are the Debye length, cyclotron frequencies, random velocities, Larmor radii, and collision frequencies for typical values of density, temperature, magnetic field, and pressure. Items 1 through 7 are self-explanatory. We shall indicate the sources of the estimates of the collision frequencies and mean-free paths.

The electron-neutral collision frequency is independent of electron temperature in Helium and is given by $\nu_{en} = 2.3 \times 10^9$ p, where p is the gas pressure in Torr.[1]

The frequencies of collisions between charged particles were calculated by using

$$\nu_{ei} = \frac{8}{3}\sqrt{\frac{\pi}{2}}\,\frac{n_e e^4 z \ln \Lambda}{\sqrt{m_e}\,(kT_e)^{3/2}} = \frac{m_i}{m_e}\,\nu_{ie}$$

and

$$\nu_{ee} = \frac{n_e \ln \Lambda}{0.266\, T_e^{3/2}} = \left(\frac{T_i}{T_e}\right)^{3/2} \nu_{ii}$$

from Spitzer.[2] The symbols in these equations have their usual meanings.

The ion-neutral collision frequency was obtained from the room-temperature mobility of He^+ in He when E/p is zero $\left(\mu_+ = 10.8\ \frac{cm^2}{sec\ V}\right)$.[3] The value for frequencies obtained in this way is an underestimate in which the variation of collision frequency with ion temperature is neglected.

Table XVIII-2. Estimates of parameters describing the helium plasma.

Quantity and Basis of Estimate	Assumed Conditions	Computed Values
1. Electron Debye length $\lambda_D = \left(kT_e/4\pi n_e e^2\right)^{1/2}$	$1\times10^{10} \leq n_e \leq 1\times10^{11}$ cm^{-3} $1 \leq T_e \leq 100$ eV	$2\times10^{-3} \leq \lambda_D \leq 7\times10^{-2}$ cm
2. Electron cyclotron frequency $\omega_{ce} = eB/m_e = 2\pi f_{ce}$	B = 1000 G	ω_{ce} = 18 GHz f_{ce} = 3 GHz
3. Ion cyclotron frequency $\omega_{ci} = eB/m_i = 2\pi f_{ci}$	B = 1000 G Helium ions	ω_{ci} = 2.4 MHz f_{ci} = 0.4 MHz
4. Electron random velocity $v_{Te} = (kT_e/m_e)^{1/2}$	$1 \leq T_e \leq 100$ eV	$4\times10^{7} \leq v_{Te} \leq 4\times10^{8}$ cm/sec
5. Ion random velocity $v_{Ti} = (kT_i/m_i)^{1/2}$	$0.1 \leq T_i \leq 5$ eV Helium ions	$5\times10^{5} \leq v_{Ti} \leq 3\times10^{6}$ cm/sec
6. Electron Larmor radius $r_{Le} = v_{Te}/\omega_{ce}$	B = 1000 G $1 \leq T_e \leq 100$ eV	$3\times10^{-3} \leq r_{Le} \leq 3\times10^{-2}$ cm
7. Ion Larmor radius $r_{Li} = v_{Ti}/\omega_{ci}$	B = 10000 G $0.1 \leq T_i \leq 5$ eV	$0.2 \leq r_{Li} \leq 1.5$ cm
8. Electron-neutral collision frequency and mean-free path	$p = 2\times10^{-5}$ Torr Helium T_e = 10 eV	$\nu_{en} = 5\times10^{4}$/sec $\lambda_{en} = 3\times10^{3}$ cm
9. Electron-ion collision frequency and mean-free path	Helium ions $n_e = 10^{11}$/cm^{-3}, T_e = 10 eV	$\nu_{ei} = 2\times10^{5}$/sec $\lambda_{ei} = 8\times10^{2}$ cm
10. Electron-electron collision frequency and mean-free path	$n_e = 10^{11}$/cm^3 T_e = 10 eV	$\nu_{ee} = 2\times10^{5}$/sec $\lambda_{ee} = 8\times10^{2}$ cm
11. Ion-ion collision frequency and mean-free path	$n_i = 10^{11}$/cm^3 T_i = 1 eV	$\nu_{ii} = 6\times10^{6}$/sec λ_{ii} = 3 cm
12. Ion-electron collision frequency and mean-free path	$n_i = n_e = 10^{11}$/cm^3 T_e = 10 eV, T_i = 1 eV	$\nu_{ie} = 3\times10^{1}$/sec $\lambda_{ie} = 2\times10^{4}$ cm
13. Ion-neutral collision frequency and mean-free path	$p = 2\times10^{-5}$ Torr T_i = 1 eV	$\nu_{in} = 6\times10^{2}$/sec $\lambda_{in} = 3\times10^{3}$ cm

Langmuir Probe Measurements

A single Langmuir probe has been used to measure the electron density, electron temperature, and space potential. We made the measurements presented here on a Helium plasma generated in PF 2, using equipment and procedures similar to those described in Section XVIII-C. 1. The plasma properties were measured as a function of position and the externally controlled plasma conditions, such as RF power, pressure, flow, and magnetic field.

The probe consists of a tungsten wire, of 2-mil diameter, insulated by a drawn-down quartz tube, except for an exposed length of approximately 2 mm. The radius of the cylindrical probe is less than the Debye length and much less than the ion Larmor radius, so that the measured probe curves can be interpreted by using the orbital theory of ion collection in the absence of a magnetic field.[4] Details of the data analysis are given in Section XVIII-A. 1. No measurements of the ion temperature were made in this case because the Helium ion emission spectrum was not detectable. It was assumed that the ion temperature in the Helium plasma was the same as in the Argon plasma, roughly 1 eV.

Figures XVIII-18, XVIII-19, and XVIII-20 show the measured radial profiles of density, temperature, and potential for various flow rates. The flow rate itself is too low to measure reliably with a conventional rotometer; instead, the pressure in the system is taken as a measure of the flow. The density is in the range 2×10^{10}-2.3×10^{11} cm^{-3}. The electron temperature range is 4-16 eV, and the potential varies between -35 V and +15 V. The measurements were made with 25 W excitation power. The main magnetic field was 1100 G, and the mirror ratio was 1. 6.

It can be seen that the profiles indicate a somewhat hollowed out cylinder of plasma, especially at the lower flow rates. The density and potential, and to a lesser extent, the electron temperature, increase to maximum values at a radius that is roughly equal to the radius of the Lisitano structure (1. 4 cm) and then fall off rather quickly at larger radii. This is in qualitative agreement with the data obtained on the PF 1 plasma without a grid, and also with the results reported by Lisitano.[5]

Increasing the flow rate has the effect of smoothing out the temperature and space potential profiles. The average temperature decreases with increasing flow, while the electron density increases substantially as the flow increases. The density profile at large radii appears to be independent of pressure. The density drop-off is quite sharp with an e-folding length of the order of, or less than, an ion Larmor radius.

Some indication of the error brackets appropriate for a single day's data can be obtained from Figs. XVIII-18 through XVIII-20. The two points for the 68. 08-cm position in the curves at 2×10^{-5} Torr pressure represent the result of repeating that probe curve near the beginning and at the end of the series of measurements. The primed

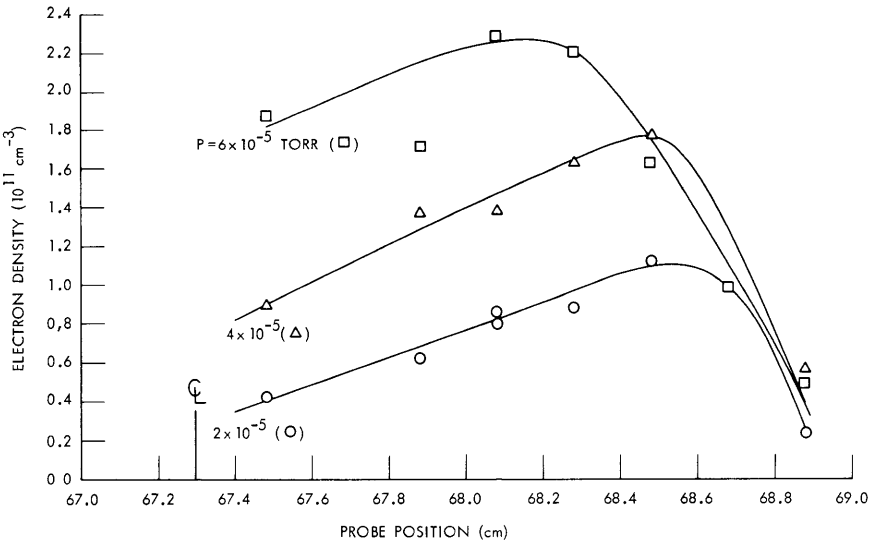

Fig. XVIII-18. Electron density vs radial position for various flow rates.

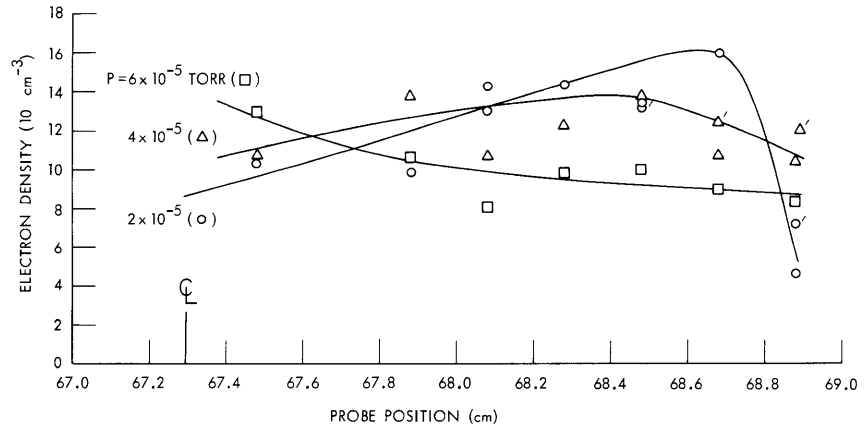

Fig. XVIII-19. Electron temperature vs radial position for various flow rates.

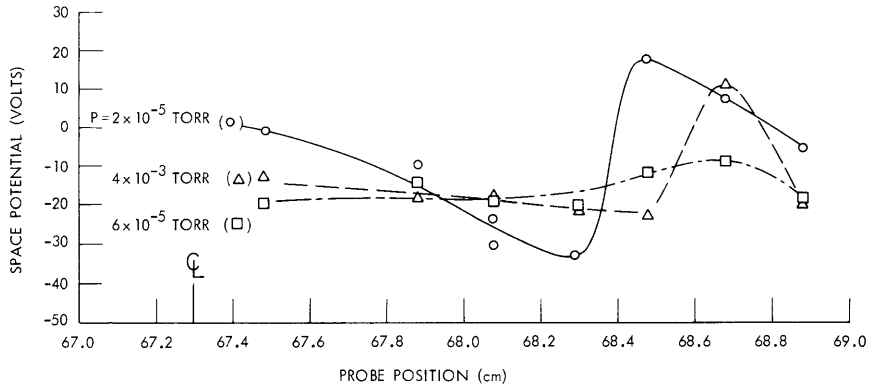

Fig. XVIII-20. Space potential vs radial position for various flow rates.

points at 2×10^{-5} and 4×10^{-5} Torr in the graphs of electron temperature and space potential vs radius show the effects of repeating only the data analysis for a given probe curve. The error brackets estimated on this basis are approximately 8% for electron density and 20% for electron temperature and space potential. A comparison of data taken on different days indicated somewhat greater differences, although the general shape of the profiles and the magnitudes of the measured quantities were reproduced.

If a potential profile is computed from the measured density and temperature profiles, with the aid of Simon diffusion theory,[6] the result does not show the two electric-field reversals seen in the low-flow experimental data. It is interesting to note that a potential profile of the observed shape can be obtained, however, from Poisson's equation for an assumed charge distribution that is physically not unreasonable. A schematic representation of the density distribution comprises a thin-walled cylinder of electrons and a thicker wall concentric cylinder of ions. The radii of the cylinders are equal to the radius of the Lisitano structure, which corresponds to the assumption that the plasma is produced near the walls of the structure. The wall thicknesses represent the Larmor radii of the two species. The ratio of the charge densities in the two cylinders makes the total charge zero, although the electron and ion densities are not equal at each point in the charge distribution. Figure XVIII-21 shows such a charge distribution and the potential obtained by graphical integration of Poisson's equation. It can be seen that the potential is qualitatively similar to that observed in the experiment.

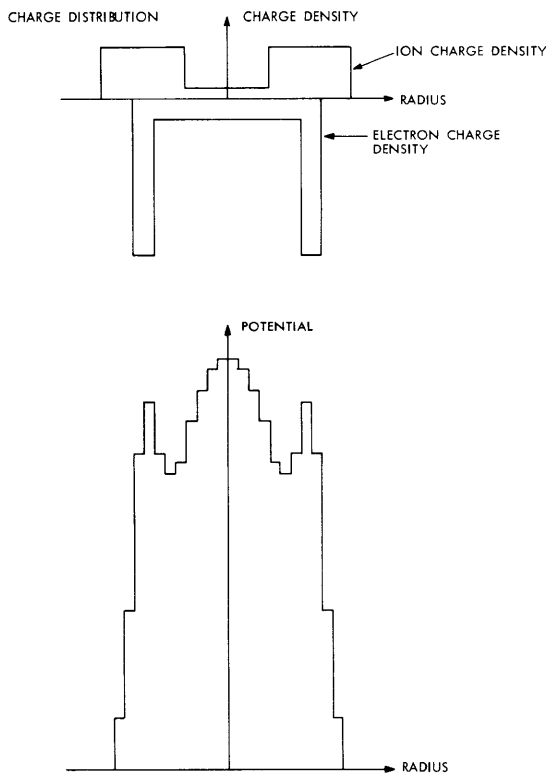

Fig. XVIII-21.
Potential distribution for assumed schematic charge distribution.

In addition to the measurements of the radial profiles of the plasma properties, the variations of the density, temperature, and potential in response to changes in the input power, gas pressure, flow, magnetic field, and mirror ratio were measured. The results of these observations are summarized in Table XVIII-3. The pressure was varied at constant flow by partially closing the normally open gate valve leading to the diffusion pump. The pressure with the gate valve open is taken as an indication of the flow rate, as noted before.

Table XVIII-3. Variation of measured plasma characteristics with external plasma conditions.

Property	RF Power Range: 14-34 W	Pressure at Constant Flow Range: 2×10^{-5}-7×10^{-5} Torr	Flow Range: Pressure 2×10^{-5}-7×10^{-5} Torr	Main Magnetic Field Range: 0.2%	Mirror Magnetic Field Range: 10%
n_e	Increases linearly with power Roughly 25 W doubles density	Proportional to pressure $<5\times10^{-5}$ Torr Saturates at higher pressure	Same as pressure	Sharp maximum Plasma extinguishes at 0.2% off optimum	Broader maximum Plasma extinguishes at 10% off optimum
T_e	Slight linear increase with power	Slight decrease (10%) with increasing pressure	Slight decrease (10%) with increasing flow	Independent	Independent
V_s	Independent	Independent	Independent	Slight decrease with increasing field	Independent

It can be seen that the electron temperature and the space potential vary liitle for the range of conditions observed. The density is very sensitive to the magnetic field and increases with increasing pressure and RF power.

Conclusion

The data presented in this report have shown that the Helium plasma generated in the PF 2 apparatus at low pressures is concentrated primarily at a radius equal to the radius of the generating microwave structure. The peak electron density is of the order of $10^{11}/cm^3$, and the peak temperature is of the order of 10-15 eV. The decrease in electron density at the edge of the plasma is quite sharp and independent of pressure. Further measurements on the Helium plasma are not planned at the present time. Future probe diagnostics will be performed in Argon in conjunction with the continuing ion temperature measurements.

J. K. Silk, E. W. Fitzgerald, G. Bekefi

References

1. S. C. Brown, Basic Data of Plasma Physics (The M.I.T. Press, Cambridge, Mass., 1959).
2. L. Spitzer, Jr. Physics of Fully Ionized Gases (Interscience Publishers, Inc., New York, 1962).
3. E. W. McDaniel, Collision Phenomena in Ionized Gases (John Wiley and Sons, Inc., New York, 1964).
4. F. F. Chen, Phys. Fluids 11, 811 (1968).
5. G. Lisitano, Proc. Seventh International Conference on Ionization Phenomena in Gases, Vol. I (Gradevinska Knjiga Publ. Houses, Beograd, 1966); G. Lisitano, R. A. Ellis, Jr., W. M. Hooke, and T. H. Stix, Plasma Physics Laboratory MATT-Q-24, Princeton University, Princeton, N.J., 1966; G. Lisitano, Appl. Phys. Letters 12, 32 (1968).
6. S. C. Brown (ed.), Electrons, Ions, and Waves – Selected Works of William Phelps Allis (The M.I.T. Press, Cambridge, Mass., 1967).

XVIII. PLASMAS AND CONTROLLED NUCLEAR FUSION*

D. Fusion-Related Studies

Academic and Research Staff

Prof. D. J. Rose
Prof. R. J. Briggs

Graduate Students

G. L. Flint, Jr.
Y. Y. Lau
A. E. Wright

RESEARCH OBJECTIVES

1. Feasibility of Pulsed Fusion Devices

A limited study of problems that would be peculiar to power systems operating via a pulsed fusion cycle was started in 1968 and will be completed in 1969. Several schemes that have been proposed will be examined analytically: Cu-Zr coils for structural integrity; coils that are lithium-cooled for heat transfer; coils plus a lithium moderator for tritium breeding; vacuum wall degradation and/or destruction during pulses. The objective is to combine all of the main components so that as many principal effects and problems can be seen at once as is possible, even though the view is very approximate.

G. L. Flint, Jr., D. J. Rose

2. Analysis of Fusion Plasma Conditions

A small analytic study of electron and ion temperatures, energy exchange rate, and other things of importance in deuterium-tritium fusion plasmas was started in 1968, and will be completed in 1969. For example, the plasma is heated in part by the thermalization of alpha-particles created in the D + T → n(14.1 MeV) + α(3.5 MeV) fusion reaction. Just how these α thermalize is hard to calculate exactly, but the effect of various limiting assumptions will be explored. Also to be studied are the effects of incomplete α-thermalization, modified electron-ion energy transfer rates, and other variations. Computational methods have been developed to treat these problems.

F. B. Marcus, D. J. Rose

3. Fuel Injection into a Fusion Device

Estimates, thus far, are that the plasma size will be very large in many economically attractive fusion power systems. This is particularly so for steady-state devices, and the question arises how fresh deutrium-tritium nuclear fuel can be injected deep into the plasma. The difficulty comes from the flux of energy in the plasma (of the order of 10^{14} W/m^2). This will reionize fast D or T atoms that are injected into the plasma, long before they penetrate far. Larger pellets will ablate, and form a high-pressure cold plasma in their vicinity. Whether such pellet injection is feasible is not

*This work was supported by the U.S. Atomic Energy Commission (Contract AT(30-1)-3980).

now known with confidence. Main effort will be directed toward pellet injection, at first analytically. Experiments utilizing very small pellets injected into available plasmas (at M. I. T. or elsewhere) may be undertaken.

A. E. Wright, D. J. Rose

4. Stability of Relativistic Electron Layers

We have begun a theoretical study of the stability of relativistic electron layers in a plasma, the primary application being the Astron Thermonuclear Experiment. Our model of the electron layer assumes concentric orbits of the particles, but is otherwise unrestricted as far as density profile is concerned and properly accounts for the finite size of the electron ring. The effects of a background plasma on the negative-mass modes will be studied in some detail during the coming year.

R. J. Briggs

1. STABILITY OF RELATIVISTIC ELECTRON RINGS

We have initiated a research program concerned with the stability of relativistic gyrating electron beams of finite thickness in the presence of background plasma. Practical applications for which this study is of interest include the Astron Thermonuclear experiment and the proposed electron ring accelerator.[1] In the initial phases,

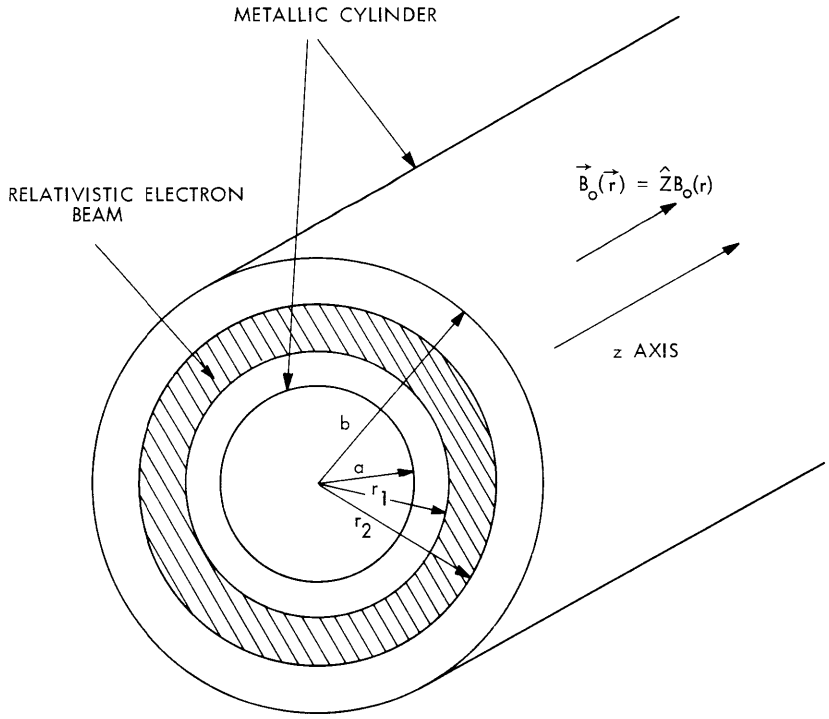

Fig. XVIII-22. The model. A layer of relativistic electrons, with density $n_o(r)$, is guided by a magnetic field $\vec{B}_o(\vec{r})$.

our main attention will be on the formulation of a model that can describe the negative-mass instability[2,3] in the Astron configuration, with particular emphasis on the effects of cold plasma on this mode.

The present analysis is based on a model that approximates the Astron configuration. The model consists of a metallic cylinder of inner radius a and outer radius b, as shown in Fig. XVIII-22. An electron beam of density $N_o(r)$, guided by a magnetic field $\vec{B}_o = B_o(r)\,\hat{Z}$, is located between $r = r_1$ and $r = r_2$. The unperturbed orbits of the electrons are concentric circles centered at the origin. Thermal effects and spread in canonical momentum are neglected. This model is clearly idealized, since, in reality, nonconcentric orbits, spread in canonical momentum, and betatron oscillations normally arise. Disorders like energy spread and nonconcentric orbits tend, however, to suppress beam instability.[4,5] Therefore, the study of instability for an ordered beam in the absence of frequency spread enables us to estimate the frequency spread required for stability.

We approach the problem first by obtaining the linearized constitutive relation for the relativistic beam, $\vec{J} = \vec{J}(\vec{E}, \vec{H})$, through the Lorentz force law and continuity equation. We then solve Maxwell's equations, including in general the plasma contribution to the total current by means of the plasma dielectric tensor. In the initial work, we shall examine the stability of the beam in vacuum.

Constitutive Relation

Consider an electron beam gyrating about the z axis with density $n_o(r)$ and beam current $\vec{J}_o(r) = \hat{\theta} J_o(r)$ guided by an axial magnetic field $\vec{B}_o = \hat{Z} B_o(r)$. The cylindrical layer is assumed to be infinite in z, and the unperturbed space charge is neutralized by immobile ions. The unperturbed velocity $\vec{v}_o = \hat{\theta} v_o(r)$ is then given by

$$\frac{v_o(r)}{r\sqrt{1 - \frac{v_o^2(r)}{c^2}}} = -\frac{e}{m_o}\left[B_o(r) + \mu_o \int_r^{r_2} J_o(r)\, dr\right].$$

The last term in this equation accounts for the self-magnetic field; the unperturbed electric field is zero by assumption.

Let

$$\omega_c(r) = -\frac{e}{m_o}\left[B_o(r) + \mu_o \int_r^{r_2} J_o(r)\, dr\right].$$

Then

$$v_o(r) = \frac{r\omega_c(r)}{\sqrt{1 + \frac{\omega_c^2 r^2}{c^2}}},$$

and the actual gyration frequency is

$$\omega_o(r) = \frac{v_o(r)}{r} = \frac{\omega_c(r)}{\gamma_o(r)},$$

where

$$\gamma_o(r) = \left(1 - \frac{v_o^2}{c^2}\right)^{-1/2}$$

is the usual relativistic factor.

Assume that the perturbed velocity $\vec{v}_1(\vec{r}, t)$ and field quantities $\vec{E}_1(\vec{r}, t)$, $\vec{H}_1(\vec{r}, t)$ have the following form:

$$\vec{v}_1(\vec{r}, t) = [\hat{r}v_r(r) + \hat{\theta}v_\theta(r)]\, e^{j\omega t - j\ell\theta}$$

$$\vec{E}_1(\vec{r}, t) = [\hat{r}E_r(r) + \hat{\theta}E_\theta(r)]\, e^{j\omega t - j\ell\theta}$$

$$\vec{H}_1(\vec{r}, t) = \hat{Z}H_Z(r)\, e^{j\omega t - j\ell\theta}.$$

It can be shown that the relativistic Lorentz force law

$$\frac{\partial}{\partial t}\left[\frac{\vec{v}}{\sqrt{1 - \frac{v^2}{c^2}}}\right] + \vec{v} \cdot \nabla\left[\frac{\vec{v}}{\sqrt{1 - \frac{v^2}{c^2}}}\right] = \frac{e}{m_o}[\vec{E} + \vec{v} \times \vec{B}]$$

can be linearized into the following equations:

$$v_r \gamma_o j(\omega - \ell\omega_o) - v_\theta \omega_o \gamma_o^3 = \frac{e}{m_o}[E_r + v_o \mu_o H_Z]$$

$$v_r \frac{dv_o}{dr} + v_\theta j(\omega - \ell\omega_o) = \frac{e}{m_o \gamma_o^3} E_\theta,$$

from which we obtain

$$v_r = \frac{\frac{e}{m_o}[j(\omega - \ell\omega_o)(E_r + \mu_o v_o H_Z) + \omega_o E_\theta]}{\gamma_o\left[\gamma_o^2 \omega_o\left(\frac{dv_o}{dr}\right) - (\omega - \ell\omega_o)^2\right]} \tag{1}$$

$$v_\theta = \frac{\frac{e}{m_o}\left[(E_r+\mu_o v_o H_Z)\frac{dv_o}{dr} - \frac{1}{\gamma_o^2} j(\omega-\ell\omega_o)\, E_\theta\right]}{\gamma_o\left[(\omega-\ell\omega_o)^2 - \gamma_o^2\omega_o\left(\frac{dv_o}{dr}\right)\right]}. \tag{2}$$

Then the linearized constitutive relation is given by

$$\vec{J}_1(\vec{r},t) = en_o\vec{v}_1 + en_1\vec{v}_o$$

$$= \hat{r}[en_o v_r] + \hat{\theta}\,\frac{en_o v_\theta j\omega - e\omega_o \frac{d}{dr}[n_o r v_r]}{j(\omega-\ell\omega_o)}. \tag{3}$$

Here, we have used the linearized continuity equation to find n_1. With (1) and (2) substituted in (3), we obtain the constitutive relation $\vec{J}_1 = \vec{J}_1(\vec{E}_1, \vec{H}_1)$. Thus far, our analysis is "exact," in the sense that no approximations about $n_o(r)$, $B_o(r)$, $\gamma_o(r)$ have yet been made.

In order to simplify the calculations, let us introduce two assumptions:

1. $\Omega \equiv \omega - \ell\omega_o \ll \omega_o$

2. $\omega_p^2 \equiv \frac{n_o(r)\, e^2}{m_o \epsilon_o \gamma_o(r)} \ll \omega_o^2$.

The first assumption implies that we are looking for longitudinal modes with $\omega \approx \ell\omega_o$, and the second is valid only when the self-magnetic field is much less than the vacuum field. With these approximations, it can be shown that the radial and azimuthal components of $\vec{J}_1$ are given by

$$J_r(r) = \frac{\omega_p^2 \epsilon_o E_\theta}{\gamma_o^2 \frac{dv_o}{dr}} \tag{4}$$

$$J_\theta(r) = \frac{j\omega_o}{\Omega}\frac{d}{dr}\left[\frac{\epsilon_o r \omega_p^2 E_\theta}{\gamma_o^2 \frac{dv_o}{dr}}\right]. \tag{5}$$

The expressions for $\vec{J}_1$ are valid as long as E_r (or, $E_r + v_o B_1$) is of the same order of magnitude as E_θ. Note also that no approximations about $B_o(r)$ and $n_o(r)$ have been made yet.

Limit of a Thin Layer

It can be shown that our analysis is consistent with that for the thin layer. The transformation

$$v_r(r) = \dot{\xi}$$

$$v_\theta(r) = \dot{\eta} + \omega_o \xi - \xi \frac{dv_o}{dr}$$

from the Eulerian coordinates to the polarization coordinates[6] shows that (1) and (2) are indeed consistent with the results of Briggs and Neil.[2] In the transformation above ξ and η are the radial and azimuthal displacement of an electron from its unperturbed orbit.

In the limit of infinitesimal thickness, E_θ is approximately continuous across the layer, and $\frac{dv_o}{dr} \approx \frac{\omega_o}{\gamma_o^2}$. Then the equivalent perturbation surface current K_θ is given by

$$K_\theta = \int_{r_1}^{r_2} J_\theta \, dr \approx \left[jr\epsilon_o \frac{\omega_p^2}{\Omega} E_\theta \right]_{r_1}^{r_2} + \beta_o^2 \epsilon_o \frac{\omega_p^2 \omega}{\Omega^2} jE_\theta \tau$$

$$= \beta_o^2 \epsilon_o \frac{\omega_p^2 \omega}{\Omega^2} jE_\theta \tau; \quad \tau \equiv r_2 - r_1, \quad \text{and} \quad \beta_o^2 = v_o^2/c^2$$

since the first term is identically equal to zero. This expression for K_θ is identical to the results of Briggs and Neil,[2] and the present derivation shows that the unperturbed profile of the beam is unimportant.

Differential Equation for the Fields

For the case of a beam in vacuum, the remainder of the task is to solve Maxwell's equations

$$\nabla \times \vec{E}_1 = -j\omega\mu_o \vec{H}_1 \tag{6}$$

$$\nabla \times \vec{H}_1 = \hat{r}(J_r + j\omega\epsilon_o E_r) + \hat{\theta}(J_\theta + j\omega\epsilon_o E_\theta), \tag{7}$$

subject to the appropriate boundary conditions. From (4), (5), and (7), we find the following differential equation for E_θ.

$$\frac{d}{dr}\left[\frac{r}{\frac{\omega^2 r^2}{c^2} - \ell^2} \left\{ \frac{d}{dr}(rE_\theta) - \frac{\ell \omega_p^2 E_\theta}{\omega \omega_o} \right\} \right] + \frac{\omega_o}{\omega\Omega} \frac{d}{dr}\left[\frac{\omega_p^2 r E_\theta}{\omega_o} \right] + E_\theta = 0. \tag{8}$$

We have assumed that $B_o(r) = B_o$ = constant (hence $\omega_c(r) = -eB_o/m_o$ and $dv_o/dr = \omega_o/\gamma_o^2$) to obtain (8).

The structure and solutions to Eq. 8 are now being studied. The analysis is complicated by the appearance in Eq. 8 of an apparent singularity at $r = \frac{\ell c}{\omega}$ in addition to the true singularity at $\omega_o(r) = \frac{\omega}{\ell}$.

Y. Y. Lau, R. J. Briggs

References

1. Symposium on Electron Ring Accelerators, Lawrence Radiation Laboratory, Berkeley, California, 1968. (UCRL 18103.)
2. R. J. Briggs and V. K. Neil, "Negative-Mass Instability in a Cylindrical Layer of Relativistic Electrons," J. Nucl. Energy, Part C, Vol. 9, pp. 207-227, 1968.
3. V. K. Neil and W. Heckrotte, "Relation between Diochotron and Negative Mass Instabilities," J. Appl. Phys. 36, 100 (1965).
4. R. Landau and V. K. Neil, "Negative Mass Instability," Phys. Fluids 9, 2412-2417 (1966).
5. A. Nocentini, H. L. Berk, and R. N. Sudan, "Kinetic Theory of Diochotron Instability," J. Plasma Phys., Vol. 2, Part 3, pp. 311-327, 1968.
6. D. L. Bobroff, "Independent Space Variable for Small-Signal Electron Beam Analysis," IRE Trans., Vol. ED-6, p. 20, November 1, 1959.